communications biology

A Nature Portfolio journal

Article

https://doi.org/10.1038/s42003-025-07755-z

Targeting NLRC5 in cardiomyocytes protects postinfarction cardiac injury by enhancing autophagy flux through the CAVIN1/CAV1 axis

Lingfeng Gu[1,6], Sibo Wang[1,6], Liuhua Zhou[1,6], Wenjing Wang[1], Yulin Bao[1], Ye He[1], Tongtong Yang[1], Jiateng Sun[1,2], Qiqi Jiang[1], Tiankai Shan[1], Chong Du[1], Zemu Wang[1], Hao Wang[1], Liping Xie[3], Aihua Gu[4], Yang Zhao[5], Yong Ji[3], Qiming Wang[1] ✉ & Liansheng Wang[1] ✉

NOD-like receptor (NLR) family proteins are implicated in various cardiovascular diseases. However, the precise role of NLRC5, the largest member of this family, in myocardial infarction (MI) remains poorly understood. This study reveals that NLRC5 is upregulated in the hearts of both patients with MI and MI mice. Silencing NLRC5 in cardiomyocytes impairs cardiac repair and functional recovery, while its overexpression enhances these processes. Furthermore, NLRC5 promotes autophagy in cardiomyocytes, and its protective effects are diminished upon autophagy inhibition. Mechanistically, NLRC5 interacts with CAVIN1, facilitating its degradation and subsequent downregulation of CAV1, which in turn increases the expression of the ATG12-ATG5 complex to stimulate autophagy. Conversely, CAV1 overexpression partially suppresses autophagy and attenuates the improvements in cardiac function observed in NLRC5-overexpressing MI hearts. This study highlights the critical regulatory role of NLRC5 in modulating cardiomyocyte autophagy flux, suggesting that NLRC5 activation may represent a promising therapeutic strategy for MI.

Ischemic heart disease affects an estimated 244.1 million individuals worldwide, leading to approximately 9.0 million deaths annually[1]. Despite significant therapeutic advancements, myocardial infarction (MI) remains the most severe and prognostically unfavorable form of ischemic heart disease. Following MI, cardiomyocytes experience various forms of cell death, and the sustained loss of these cells severely impairs cardiac function, contributing to heart failure or sudden death[2–4]. Consequently, preserving cardiac function amidst cardiomyocyte loss is critical for improving post-MI outcomes.

Macroautophagy (henceforth referred to as autophagy) is a vital subcellular process that occurs under both basal and stress conditions. In the heart, autophagy plays a pivotal role in maintaining myocardial homeostasis by degrading dysfunctional cytoplasmic components through the formation of autophagosomes, double-membraned vesicles that ultimately fuse with lysosomes for cargo degradation[5,6]. Previous studies have demonstrated that genetic ablation or pharmacological inhibition of autophagy in mouse models of myocardial ischemia and MI exacerbates cardiac dysfunction[7–9]. Conversely, activation of autophagy attenuates ischemia-induced myocardial damage[10–13]. However, the molecular mechanisms driving autophagy activation following MI remain poorly understood.

Nucleotide-binding oligomerization domain (NOD)-like receptors (NLRs) are recognized as essential regulators of various cellular processes, including autophagy[14]. NLRs typically consist of an N-terminal caspase recruitment domain (CARD), a central NACHT domain (a nucleoside triphosphatase domain), and a C-terminal leucine-rich repeat (LRR) domain. Among NLR family members, NLR family CARD domain-

[1]Department of Cardiology, The First Affiliated Hospital of Nanjing Medical University, 300 Guangzhou Road, Nanjing, 210029, China. [2]Department of Cardiology, Drum Tower Hospital, Medical School of Nanjing University, 321 Zhongshan Road, Nanjing, 210008, China. [3]Key Laboratory of Cardiovascular and Cerebrovascular Medicine, Key Laboratory of Targeted Intervention of Cardiovascular Disease, Collaborative Innovation Center for Cardiovascular Disease Translational Medicine, Nanjing Medical University, 101 Longmian Avenue, Nanjing, 211166, China. [4]State Key Laboratory of Reproductive Medicine, School of Public Health, Nanjing Medical University, 101 Longmian Avenue, Nanjing, 211166, China. [5]Department of Biostatistics, School of Public Health, China International Cooperation Center for Environment and Human Health, Nanjing Medical University, 101 Longmian Avenue, Nanjing, 211166, China. [6]These authors contributed equally: Lingfeng Gu, Sibo Wang, Liuhua Zhou. ✉e-mail: wangqiming@jsph.org.cn; drlswang@njmu.edu.cn

containing 5 (NLRC5) has been extensively studied for its role in antigen presentation and inflammation[15,16]. Recent studies also suggest that NLRC5 may regulate autophagy in cancer, viral infections, and liver diseases[17–19]. However, its specific role and underlying mechanisms in the context of MI, particularly with respect to cardiomyocyte autophagy, remain largely unexplored.

This study aims to investigate the therapeutic potential of targeting NLRC5 to modulate autophagy and improve cardiac function post-MI. The objectives are: (1) to determine whether NLRC5 is activated in cardiomyocytes following ischemic injury; (2) to elucidate the role of NLRC5 in MI pathophysiology; (3) to assess whether NLRC5 modulates cardiomyocyte autophagy and cardiac function after MI; and (4) to investigate the mechanisms by which NLRC5 regulates autophagy in cardiomyocytes during ischemic injury, both in vitro and in vivo.

Results

NLRC5 is upregulated in infarcted myocardium and downregulation of NLRC5 in cardiomyocyte aggravates cardiac dysfunction in mice post-MI

The changes in NLRC5 levels following MI were first assessed. Analysis of the human myocardial infarction multi-omic database[20] revealed a significant increase in NLRC5 mRNA levels in ischemic and border zone cardiomyocytes compared to non-infarcted cardiomyocytes in human heart samples (Fig. 1a). Elevated NLRC5 levels were also observed in fibroblasts post-MI, whereas a reduction was noted in endothelial cells, and no significant changes were found in myeloid cells (Supplementary Fig. 1a). To further investigate the role of NLRC5 in MI, a murine model of MI was established, and immunofluorescence (IF) was used to examine the expression of NLRC5 across different cardiac cell types. Compared to sham controls, a significant increase in NLRC5 expression was observed in cardiomyocytes of the infarcted myocardium. A slight increase in NLRC5 was also noted in fibroblasts, while endothelial cells and macrophages exhibited no notable changes (Supplementary Fig. 1b). Western blot (WB) analysis demonstrated that NLRC5 protein levels were significantly elevated at 1 day post-infarction (dpi), persisted through 3 and 7 dpi, and gradually decreased by 28 dpi in infarct border zone tissue lysates of MI mice compared to controls (Fig. 1b). In vitro, ischemic stress was simulated in the AC16 human cardiomyocyte cell line using oxygen-glucose deprivation (OGD), which induced an increase in NLRC5 expression (Fig. 1c). Similarly, OGD increased NLRC5 expression in neonatal mouse cardiomyocytes (NMCMs) at both the protein and mRNA levels (Fig. 1d, e).

Given the upregulation of NLRC5 in infarcted hearts, its potential role in MI pathogenesis was investigated. Cardiomyocyte-targeted NLRC5 knockdown was achieved using adenoviral shRNA (Ad5-cTnT-NLRC5i) to assess the effects of NLRC5 inhibition during MI. Adult mice underwent MI surgery and were immediately injected with Ad5-cTnT-NLRC5i into the infarct border zone. Control mice received injections of an adenoviral vector (Ad5-Ctrli) (Fig. 1f). NLRC5 knockdown in peri-infarct cardiomyocytes, but not in non-cardiomyocytes, was confirmed by WB and IF, with a sustained reduction in NLRC5 expression observed in the Ad5-cTnT-NLRC5i group compared to controls (Fig. 1g, Supplementary Fig. 2a). Serial echocardiographic evaluations of cardiac function revealed that NLRC5 knockdown led to significant impairment in heart function, as evidenced by decreased ejection fraction (EF) and fractional shortening (FS) (Fig. 1h, i). Additionally, increased left ventricular internal diameters (internal diameter at end-diastole [LVID; d], left ventricular internal diameter at end-systole [LVID; s]) indicated greater left ventricular dilation in the NLRC5-deficient mice (Fig. 1i). Infarct size was markedly larger in NLRC5 knockdown mice at one week post-MI, as determined by Triphenyltetrazolium chloride (TTC) staining (Fig. 1j). Masson trichrome staining at four weeks post-MI revealed increased regional scar area and reduced ventricular wall thickness in the NLRC5 knockdown group (Fig. 1k). Collectively, these results demonstrate that NLRC5 is upregulated in the post-infarct myocardium and that its downregulation exacerbates cardiac dysfunction, enlarges the infarct area, and accelerates cardiac remodeling following MI.

Cardiomyocyte NLRC5 overexpression promotes cardiac function recovery in mice after MI

Following the observation that NLRC5 knockdown resulted in impaired cardiac function post-MI, the potential for cardiomyocyte-targeted NLRC5 overexpression to protect the myocardium from ischemic stress was next investigated using a cardiomyocyte-targeted adenoviral vector encoding mouse NLRC5 (Ad5-cTnT-NLRC5) (Fig. 2a). Successful NLRC5 overexpression was first confirmed through WB and IF following MI (Fig. 2b, Supplementary Fig. 2b). Echocardiographic assessments revealed that NLRC5 overexpression led to significant improvements in EF and FS, along with reductions in LVID; d, LVID; s compared to control mice (Fig. 2c–e). One week post-MI, infarct size was significantly smaller in the NLRC5-overexpressing group relative to controls (Fig. 2f). Additionally, at four weeks post-MI, NLRC5-overexpressing mice exhibited reduced regional scar area as observed by Masson trichrome staining (Fig. 2g). Quantitative reverse transcription PCR (RT-PCR) analyses demonstrated significant downregulation of fibrosis-related genes, including *Col1a1* (collagen-1), *Col3a1* (collagen-3), and *Mmp2* (matrix metalloproteinase-2), suggesting attenuated fibrotic remodeling in these mice (Fig. 2h). Furthermore, the mRNA levels of inflammatory markers *Il-6* and *Tnf-α* were decreased in the NLRC5-overexpressing group (Supplementary Fig. 3a). Histological examination revealed a reduction in the cross-sectional area of cardiomyocytes in the infarct border zone in the NLRC5-overexpressing mice when compared to controls (Fig. 2i). No significant differences were observed between the two groups in terms of survival rate, heart weight/body weight ratio, or lung weight/body weight ratio at four weeks post-infarction (Fig. 2j, Supplementary Fig. 3b, c). Collectively, these results suggest that NLRC5 plays a critical role in preserving viable myocardium after MI and provides protective effects against cardiac dysfunction and remodeling induced by ischemic injury.

NLRC5 promotes autophagy flux in cardiomyocytes following OGD

To evaluate the in vitro effects of NLRC5 targeting, an OGD model was employed to simulate myocardial injury. Adenoviral transfection efficiency was first confirmed in NMCMs but not in neonatal mouse cardiac fibroblasts (NMCFs) under both normal and OGD conditions, using quantitative RT-PCR and WB analysis (Supplementary Fig. 4a, b). Alterations in NLRC5 expression under normal conditions did not significantly impact cardiomyocyte viability (Supplementary Fig. 5a). However, NLRC5 knockdown exacerbated cardiomyocyte death, while NLRC5 overexpression protected against cell death under OGD stimulation, consistent with in vivo findings (Supplementary Fig. 5b). Given the observed increase in NLRC5 expression during ischemic stress and the impaired cardiac function in NLRC5 knockdown mice, combined with the established link between autophagy and cell survival post-MI[9,10,21], the role of NLRC5 in autophagy was further explored. RNA-seq data from the GSE206281 dataset, which included hearts from 6 infarcted and 3 non-infarcted mice, revealed a positive correlation between NLRC5 expression and autophagy markers (Supplementary Fig. 5c). WB analysis confirmed that NLRC5 overexpression promoted autophagy in NMCMs, as indicated by increased levels of Beclin-1 and LC3-II proteins, both established markers of autophagy, along with reduced levels of p62, a substrate of autophagy (Fig. 3a). Conversely, NLRC5 knockdown inhibited autophagy in cardiomyocytes (Supplementary Fig. 6a, b). Moreover, NLRC5 overexpression further enhanced autophagy in NMCMs subjected to OGD (Fig. 3b). To differentiate between the activation of autophagic flux and the downstream blockade of autophagosome processing as potential causes for increased LC3-II levels, cells were treated with bafilomycin A1, a lysosomal acidification inhibitor that impedes autophagic turnover[22]. Following bafilomycin A1 treatment, NMCMs overexpressing NLRC5 exhibited higher LC3-II levels compared to control cells (Fig. 3c), suggesting that the elevated

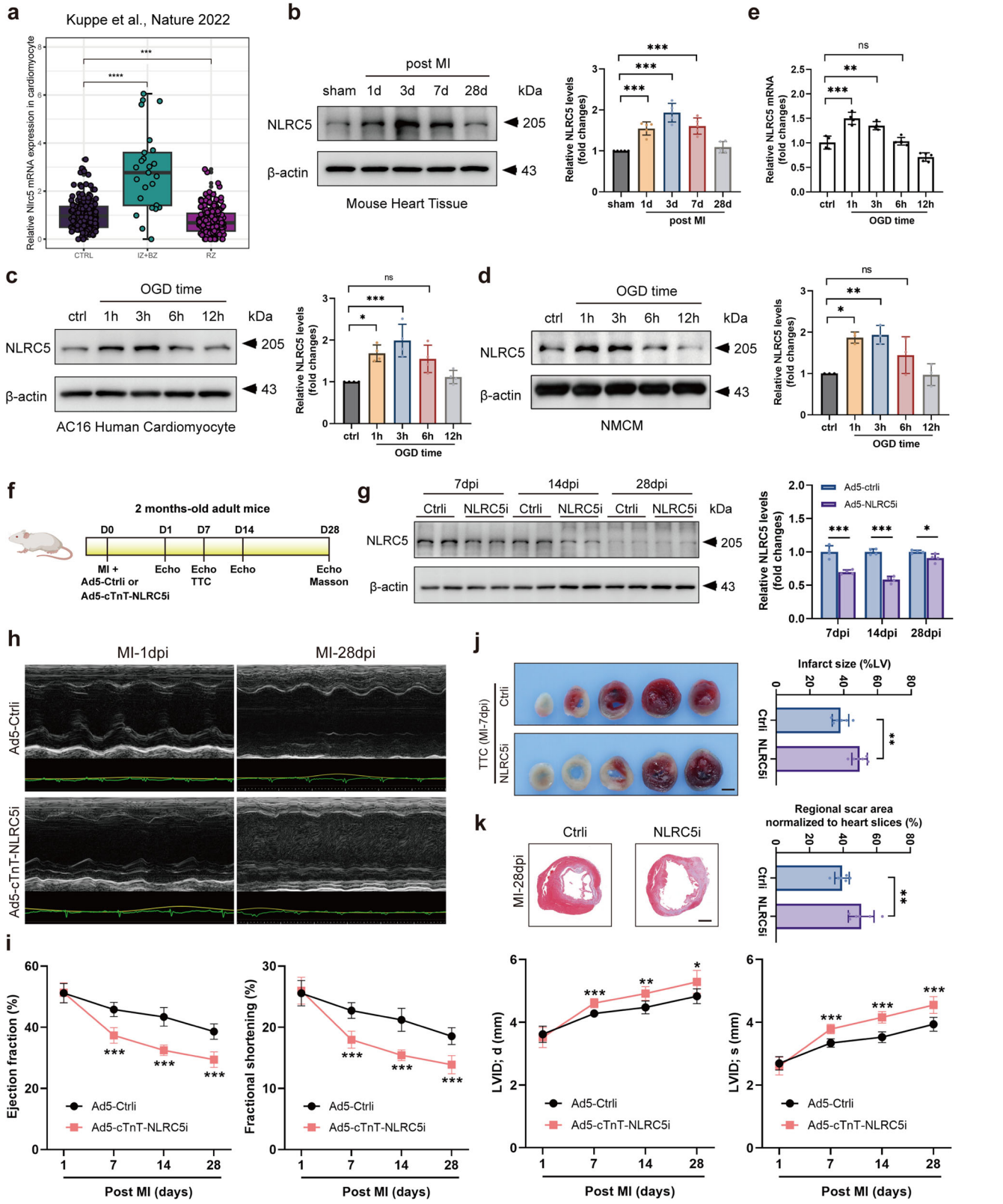

LC3-II levels were attributed to increased autophagic flux rather than impaired autophagosome turnover.

Additionally, a tandem mCherry-EGFP-LC3 probe, which enables pH-dependent visualization of autophagosomes and autolysosomes, was used to validate these observations under OGD conditions. NLRC5 overexpression resulted in an increase in both red puncta (mCherry+GFP-, representing autolysosomes) and yellow puncta (mCherry+GFP+, representing autophagosomes) per cell, along with an elevated autolysosome/autophagosome ratio, suggesting enhanced autophagic flux (Fig. 3d–f). Treatment with bafilomycin A1 induced a marked accumulation of yellow puncta and a reduction in red puncta in both control and NLRC5-overexpressing NMCMs, with the NLRC5 overexpression group exhibiting

Fig. 1 | NLRC5 is upregulated in MI cardiomyocytes and its cardiomyocyte knockdown leads to enlarged infarct size and worsened cardiac dysfunction. **a** Boxplot showing NLRC5 expression in cardiomyocytes at different sites of the infarcted heart in the human multi-omics database. IZ indicates Ischemic Zone, BZ indicates Border Zone, and RZ indicates Remote Zone. **b** Western blot and quantification of NLRC5 expression levels in border zone heart tissue lysates from mice at different time points post-MI ($n = 5$ each). **c** Western blot and quantification of NLRC5 expression in AC16 human cardiomyocytes undergoing oxygen-glucose deprivation (OGD) treatment at different time points ($n = 4$ each). **d** Western blot and quantification of NLRC5 expression in neonatal mouse cardiomyocytes (NMCMs) undergoing OGD treatment at different time points ($n = 3$ each). **e** Quantitative RT-PCR analysis and quantification of *Nlrc5* mRNA levels in NMCMs undergoing OGD treatment at different time points, with *Actb* as a control ($n = 4$-5 each). **f** The experimental timeline for the MI model. Vehicle (Ad5-Ctrli) or Ad5-cTnT-NLRC5i were injected to peri-infarct myocardium of adult mice during MI surgery. Echocardiographic analyses were performed at day (D) 1, D7, D14, and D28 post-MI (dpi). Hearts were harvested at 7, 14, and 28 dpi for histological analyses. **g** Western blot and quantification of NLRC5 in border zone heart tissue lysates from MI mice treated with Ad5-Ctrli or Ad5-cTnT-NLRC5i at 7, 14, and 28 dpi ($n = 4$ each). **h** Representative echocardiographic images of MI mice treated with Ad5-Ctrli or Ad5-cTnT-NLRC5i at 1 and 28 dpi. **i** Quantitative analysis of LVEF, LVFS, LVID;d, and LVID;s in MI mice treated with Ad5-Ctrli or Ad5-cTnT-NLRC5i at 1, 7, 14, and 28 dpi ($n = 8$ per group). **j** Infarct area in Ad5-Ctrli and Ad5-cTnT-NLRC5i treated hearts presented by triphenyltetrazolium chloride (TTC) staining of heart tissues at 7 dpi and corresponding quantification ($n = 6$ each). Scale bar, 2 mm. **k** Regional scar area in Ad5-Ctrli and Ad5-cTnT-NLRC5i treated hearts shown by Masson trichrome staining of heart tissue sections at 28 dpi and corresponding quantification ($n = 6$ each). Scale bar, 1 mm. Data are presented as mean ± SD. **a** Group-wise Mann-Whitney test. **b**-**e** 1-way ANOVA with Tukey multiple comparisons test. **g**, **j**, **k** Standard unpaired Student *t* test. **i** two-way repeated-measure ANOVA with Sidak post-hoc test. $^{*}P < 0.05$, $^{**}P < 0.01$, and $^{***}P < 0.001$. ns indicates not significant.

a greater number of puncta (Fig. 3d–f). In contrast, NLRC5 knockdown resulted in a diminished autophagic flux, evidenced by decreased red and yellow puncta and a reduced autolysosome/autophagosome ratio (Supplementary Fig. 6c–e). Finally, transmission electron microscopy (TEM) was employed to directly observe autophagic vesicle structures. The number of autolysosomes and autophagosomes was significantly higher in the OGD + NLRC5 group compared to the OGD+Ctrl group (Fig. 3g), further corroborating the results from the tandem LC3 probe experiments. Taken together, these data demonstrate that NLRC5 overexpression stimulates autophagy and enhances autophagic flux in NMCMs both under basal conditions and in the context of OGD.

The protective effect of NLRC5 toward MI injury is mediated by autophagy activation in vivo

The potential of NLRC5 to protect ischemic myocardium by activating cardiomyocyte autophagy in vivo was further explored. Initially, sham and MI models were established, and autophagy levels in the sham left ventricular cardiac tissues, as well as the infarct border zone, were evaluated in mice injected with either Ad5-cTnT-NLRC5 or Ad5-cTnT-ctrl. As anticipated, NLRC5 overexpression enhanced autophagy in the peri-infarct myocardium, as demonstrated by increased Beclin-1 and LC3-II levels, accompanied by a reduction in p62 levels at 14 days post-infarction (Fig. 4a). IF analysis revealed a notable decrease in p62 puncta in the infarct border zone cardiomyocytes of MI mice overexpressing NLRC5 (Fig. 4b). TEM further corroborated these results, showing a higher number of autophagic vesicles in the NLRC5 overexpression group compared to the control group (Fig. 4c). To further assess the role of autophagy in NLRC5-mediated cardioprotection, the effects of NLRC5 overexpression in MI mice were evaluated in the presence or absence of chloroquine (CQ), an autophagy inhibitor (Fig. 4d). WB analysis revealed that NLRC5 overexpression promoted cardiac autophagy flux, as evidenced by increased LC3-II levels. However, CQ treatment effectively impaired NLRC5-induced autophagy, as indicated by alterations in Beclin-1 and p62 levels in the MI hearts (Fig. 4e). The cardioprotective effect of NLRC5 overexpression was also attenuated in MI mice treated with CQ (Fig. 4f–h). These results collectively suggest that NLRC5 overexpression mitigates MI injury through an autophagy-dependent mechanism in vivo.

NLRC5 interacts with CAVIN1 and promotes its proteasomal degradation

To further elucidate the molecular mechanism underlying NLRC5-mediated autophagy regulation in cardiomyocytes, immunoprecipitation-mass spectrometry (IP-MS) was employed to identify potential downstream targets of NLRC5. The mass spectrometry results suggested a binding interaction between NLRC5 and CAVIN1, which was subsequently validated through co-immunoprecipitation (Co-IP), WB, and IF assays (Fig. 5a–c, Supplementary Fig. 7a). To further delineate the nature of this interaction, truncated plasmids were generated based on the amino acid (aa) sequence alignment of CAVIN1's two major structural domains: helical region 1 (HR1; 45–155 aa) and helical region 2 (HR2; 191–306 aa), alongside a full-length CAVIN1 construct (1–392 aa) (Fig. 5d). Protein truncation mapping in 293T cells revealed that NLRC5 specifically interacts with the HR1 domain of CAVIN1 (Fig. 5e), consistent with the interaction model predicted by the ClusPro server (Fig. 5f). Additionally, truncated versions of NLRC5, encompassing the CARD (1–222 aa), NAHCT (223–542 aa), and LRR (543–1915 aa) domains, as well as full-length NLRC5 (1–1915 aa), were generated to identify the specific region of NLRC5 involved in the interaction. Co-IP experiments indicated that the NAHCT domain of NLRC5 interacts with CAVIN1 (Supplementary Fig. 7b, c).

Given that NLRC5 binds to CAVIN1, this study investigated whether NLRC5 overexpression alters CAVIN1 expression in cardiomyocytes. Notably, NLRC5 overexpression significantly downregulated CAVIN1 expression in NMCMs (Fig. 5g). However, no changes were observed in *Cavin1* mRNA levels, and data from GSE206281 revealed no significant correlation between *Nlrc5* and *Cavin1* mRNA expression (Fig. 5h, Supplementary Fig. 5d), suggesting that NLRC5 regulates CAVIN1 expression post-translationally. To explore whether NLRC5 influences CAVIN1 expression through modulation of protein stability, NMCMs were treated with cycloheximide (CHX), a protein synthesis inhibitor[23], to block new protein translation. This treatment resulted in a significant reduction in CAVIN1 protein levels in NMCMs (Supplementary Fig. 8a, b). Notably, NLRC5 overexpression enhanced this effect (Supplementary Fig. 8c). Time-course analysis revealed that NLRC5 knockdown in NMCMs significantly extended the half-life of the CAVIN1 protein in the presence of CHX (Fig. 5i), suggesting that NLRC5 regulates CAVIN1 protein stability. To investigate the specific pathway through which NLRC5 regulates CAVIN1 protein stability, NMCMs were treated with CHX in the presence of lysosome inhibitors (bafilomycin A1 or E64d) or a proteasome inhibitor (MG-132). The results showed that CAVIN1 protein levels were unaffected by bafilomycin A1 or E64d, whereas a significant increase in CAVIN1 levels was observed upon treatment with MG-132 (Fig. 5j). Furthermore, MG-132, but not bafilomycin A1, rescued the NLRC5-induced reduction in CAVIN1 protein levels, indicating that NLRC5 regulates CAVIN1 stability through a proteasomal degradation pathway (Fig. 5k).

The CAVIN1/CAV1 axis mediates the effects of NLRC5 on autophagy and cardioprotection

NLRC5 modulates the stability of CAVIN1, and both CAVIN1 and its associated protein CAV1 are pivotal regulators of autophagy. To assess whether NLRC5's effects on autophagy and cardioprotection are mediated through the CAVIN1/CAV1 axis, CAVIN1 expression was downregulated using small interfering RNA (si-CAVIN1) in NMCMs. WB analysis revealed that CAVIN1 knockdown promoted autophagy (Fig. 6a, b). Moreover, LC3-II levels were significantly elevated in the si-CAVIN1 group compared to controls under OGD and bafilomycin A1 treatment, indicating enhanced autophagic flux in NMCMs subjected to OGD (Fig. 6c, d).

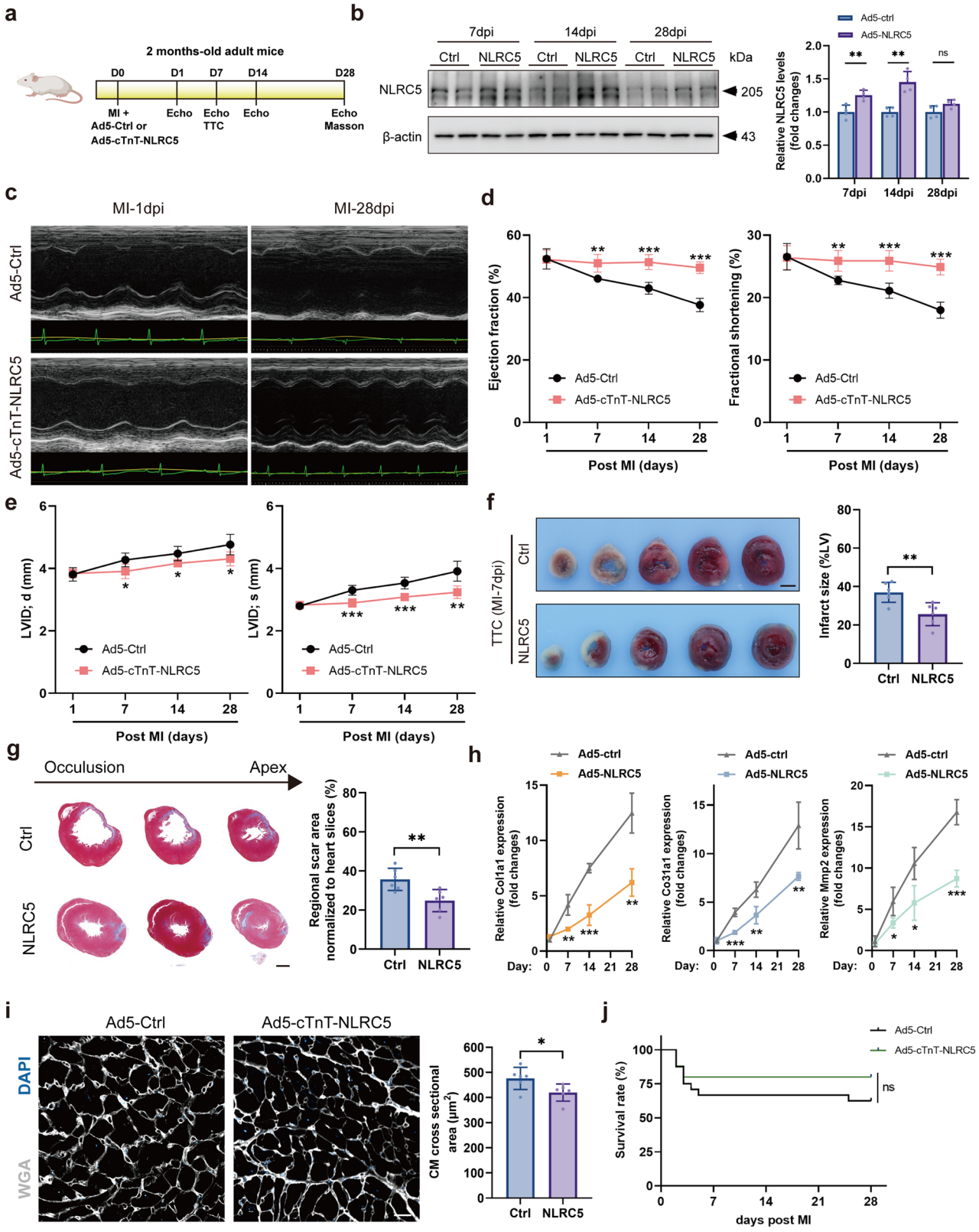

Additionally, CAVIN1 knockdown resulted in a marked increase in both yellow and red-only puncta, as well as a higher autolysosome/autophagosome ratio in NMCMs treated with the tandem fluorescent LC3 probe (Fig. 6i–k), further supporting the promotion of autophagic flux. These findings are consistent with previous observations in endothelial cells and fibroblasts[24,25], underscoring the essential role of CAVIN1 in regulating autophagic flux across diverse cell types. To further elucidate the role of CAVIN1 in NLRC5-mediated autophagy, CAVIN1 was downregulated in the context of NLRC5 knockdown. This approach revealed that CAVIN1 knockdown counteracted the inhibitory effects of NLRC5 knockdown on autophagy (Fig. 6e, f). Moreover, cell viability assessments demonstrated that CAVIN1 knockdown reversed the reduced survival associated with NLRC5 knockdown under OGD (Supplementary Fig. 9a).

Fig. 2 | Cardiomyocyte NLRC5 overexpression improves cardiac function and reduces infarct size in mice after MI. a The experimental timeline for the MI model. Vehicle (Ad5-Ctrl) or Ad5-cTnT-NLRC5 was injected to peri-infarct myocardium of adult mice during MI surgery. Echocardiographic analyses were performed at day (D) 1, D7, D14, and D28 post-MI (dpi). Hearts were harvested at 7, 14, and 28 dpi for histological analyses. **b** Western blot and quantification of NLRC5 in border zone heart tissue lysates from MI mice treated with Ad5-Ctrl or Ad5-cTnT-NLRC5 at 7, 14, and 28 dpi ($n = 4$ each). **c** Representative echocardiographic images of MI mice treated with Ad5-Ctrl or Ad5-cTnT-NLRC5 at 1 and 28 dpi. **d, e**, Quantitative analysis of LVEF, LVFS, LVID;d, and LVID;s in MI mice treated with Ad5-Ctrl or Ad5-cTnT-NLRC5 at 1, 7, 14, and 28 dpi ($n = 8$ per group). **f** Infarct area in Ad5-Ctrl and Ad5-cTnT-NLRC5 treated hearts presented by triphenyltetrazolium chloride (TTC) staining of heart tissues at 7 dpi and corresponding quantification ($n = 6$ each). Scale bar, 2 mm. **g** Regional scar area in Ad5-ctrl or Ad5-cTnT-NLRC5 treated hearts shown by Masson trichrome staining of heart tissue sections at 28 dpi and corresponding quantification ($n = 6$ each). Scale bar, 1 mm. **h** *Col1a1*, *Col3a1*, and *Mmp2* mRNA levels were detected by quantitative RT-PCR in the infarct zone of hearts transfected with Ad5-Ctrl or Ad5-cTnT-NLRC5 at 1, 7, 14, and 28 dpi ($n = 4$). **i** The CM cross sectional area in Ad5-ctrl or Ad5-cTnT-NLRC5 treated hearts at 28dpi was detected by wheat germ agglutinin (WGA) staining ($n = 6$ each). **j** Kaplan-Meier survival analysis of MI mice treated with Ad5-Ctrl or Ad5-cTnT-NLRC5 at 28 dpi (Ctrl group: $n = 24$ mice at 1 dpi and $n = 15$ mice at 28 dpi; NLRC5 group: $n = 25$ mice at 1 dpi and $n = 20$ mice at 28 dpi). Data are presented as mean ± SD. **b, f-i** Standard unpaired Student *t* test. **d, e** two-way repeated-measure ANOVA with Sidak post-hoc test. **j** Log-rank (Mantel-Cox) test. $^{*}P < 0.05$, $^{**}P < 0.01$, and $^{***}P < 0.001$. ns indicates not significant.

Accumulating evidence suggests a parallel expression pattern between CAVIN1 and CAV1[24–26]. In the present study, CAVIN1 knockdown resulted in a concomitant downregulation of CAV1 in NMCMs (Fig. 6a, b). Notably, NLRC5 overexpression also significantly decreased CAV1 levels both in hearts post-MI (Supplementary Fig. 9b, c) and in NMCMs (Supplementary Fig. 9d, e). To further investigate the role of CAV1 in autophagy, CAV1 was silenced in NMCMs using siRNA. CAV1 knockdown promoted autophagy and enhanced autophagic flux (Fig. 6g, h), an effect corroborated by tandem fluorescent LC3 probe experiments (Fig. 6i–k). To explore the underlying mechanisms of the enhanced autophagy observed upon CAV1 knockdown, the effects of CAV1 silencing on the mTOR and AMPK signaling pathways—two key regulators of autophagy, were assessed. However, no significant modulation of mTOR or AMPK activity was observed upon CAV1 silencing (Supplementary Fig. 10). Previous studies have suggested that CAV1 can modulate the expression of autophagy-related proteins (ATG), such as ATG12-ATG5 in lung epithelial cells[27]. In this study, CAV1 knockdown was found to enhance the expression of both ATG12-ATG5 and free ATG5 protein levels in NMCMs (Fig. 6l), indicating that CAV1 regulation of autophagy may occur through modulation of ATG protein expression rather than through mTOR or AMPK signaling. Consistent with this, NLRC5-mediated CAV1 knockdown also resulted in increased levels of ATG12-ATG5 (Fig. 6m).

To further elucidate the role of CAV1 in NLRC5-induced autophagy in vivo, additional experiments were conducted. WB analysis revealed that CAV1 overexpression partially attenuated the autophagic activation induced by NLRC5 overexpression, as evidenced by decreased LC3-II and ATG12-ATG5 levels, along with increased p62 levels (Fig. 7a). Four weeks after MI surgery, mice with NLRC5 overexpression exhibited higher EF and FS, smaller LVID; d and LVID; s, and reduced regional scar area compared to the Ad5-ctrl group. However, these beneficial effects were partially reversed by CAV1 overexpression (Fig. 7b–d). Taken together, these results demonstrate that the CAVIN1/CAV1 axis mediates the autophagic and cardioprotective effects of NLRC5 overexpression.

Discussion

This study presents evidence that NLRC5 plays a protective role in ischemic myocardium and acts as a key regulator of autophagy in cardiomyocytes following ischemic injury. Notably, the cardioprotective effects of NLRC5 in MI mice were significantly reduced under conditions of autophagy inhibition, suggesting that NLRC5 mediates its beneficial effects primarily through the activation of autophagy. Mechanistically, NLRC5 directly interacts with CAVIN1, promoting its proteasomal degradation, which in turn downregulates CAV1 and induces the expression of ATG12-ATG5. This enhanced autophagic flux subsequently protects cardiomyocytes, contributing to improved cardiac function in MI mice with NLRC5 overexpression, as depicted in Fig. 7e.

Our study first observed an upregulation of NLRC5 expression both in vivo and in vitro following MI, a pattern consistent with NLRC5 expression in other ischemic organs, such as the liver and kidneys[28,29]. Additionally, overexpression of NLRC5 in the myocardium under ischemic stress was found to be cardioprotective. Knockdown of NLRC5 in cardiomyocytes exacerbated cardiac dysfunction and increased regional scar area post-MI, while enhancement of NLRC5 expression in cardiomyocytes protected against ischemia-induced cell death and cardiac remodeling, highlighting NLRC5's essential role in cardiomyocyte survival during MI injury. Additionally, previous studies demonstrated that macrophage-specific NLRC5 overexpression can attenuate pressure overload-induced cardiac remodeling[30]. Thus, the present findings underscore NLRC5's critical involvement in various cardiovascular diseases. However, some published studies suggest a potentially detrimental role for NLRC5 as a pro-fibrotic regulator in both the heart[31,32] and other organs[33,34]. In contrast, our study demonstrated that NLRC5 overexpression in cardiomyocytes intended to reduce regional scar area in the MI myocardium. This discrepancy may arise from differences in the cell types and disease contexts investigated. While our study focused on cardiomyocytes, previous studies investigated fibroblasts. In support of our findings, another study suggested that NLRC5 knockout could exacerbate fibrosis in LPS-induced cardiac muscle cells in vitro[35]. The underlying reasons for these differing results remain unclear, and further investigation is warranted. Another example of this complexity is the observed dual role of NLRC5 in modulating immune responses. While NLRC5 can interact with RIG-I and MDA5 to suppress interferon (IFN) responses in 293T or RAW264.7 cells[16], it can also induce an IFN-dependent antiviral response in HeLaS3 cells[36]. These observations indicate that the effects of NLRC5 may be cell- and context-specific, further highlighting the complexity of NLRC5's role in cardiovascular and immune regulation.

Under physiological and pathological conditions, autophagy plays a pivotal role in maintaining cardiac homeostasis. Deficient autophagy shortly after birth in mice leads to ST-segment elevation in the heart[37], while its absence in adult hearts results in heart failure[38]. In contrast, enhancing autophagic activity has been shown to provide protection against age-related and ischemia-induced cardiac dysfunction[9,39]. In the current study, NLRC5 knockdown was found to significantly impair autophagy, whereas its overexpression promoted autophagic flux in cardiomyocytes under ischemic stress. Additionally, modulation of NLRC5 levels under normal conditions was also shown to impact autophagy in NMCMs. These results provide experimental evidence for NLRC5's role in modulating autophagy in cardiomyocytes. Moreover, the autophagy inhibitor CQ suppressed autophagic activity and abrogated the protective effect of NLRC5 overexpression, suggesting that the cardioprotective effects of NLRC5 are mediated, at least in part, through the activation of autophagy.

Further investigation revealed that NLRC5 regulates autophagy in cardiomyocytes via the CAVIN1-CAV1-ATG12-ATG5 axis. CAVIN1, a cytoplasmic protein expressed ubiquitously across tissues, is closely correlated with CAV1 expression and plays a key role in the formation of caveolae and the regulation of autophagy[24,25,40]. Prior studies have identified several binding partners of CAVIN1, including nuclear factor erythroid 2-related factor 2 (NRF2) and caveolae-associated proteins[25,41]. In this context, NLRC5 was identified as a novel interacting partner of CAVIN1 in cardiomyocytes, promoting its proteasomal degradation. This interaction was further validated in a human cell line (HEK-293T cells), where the HR1 domain of CAVIN1 was confirmed as the major binding site for NLRC5[42,43]. The HR1 domain, which contains a phosphoinositide lipid-binding region,

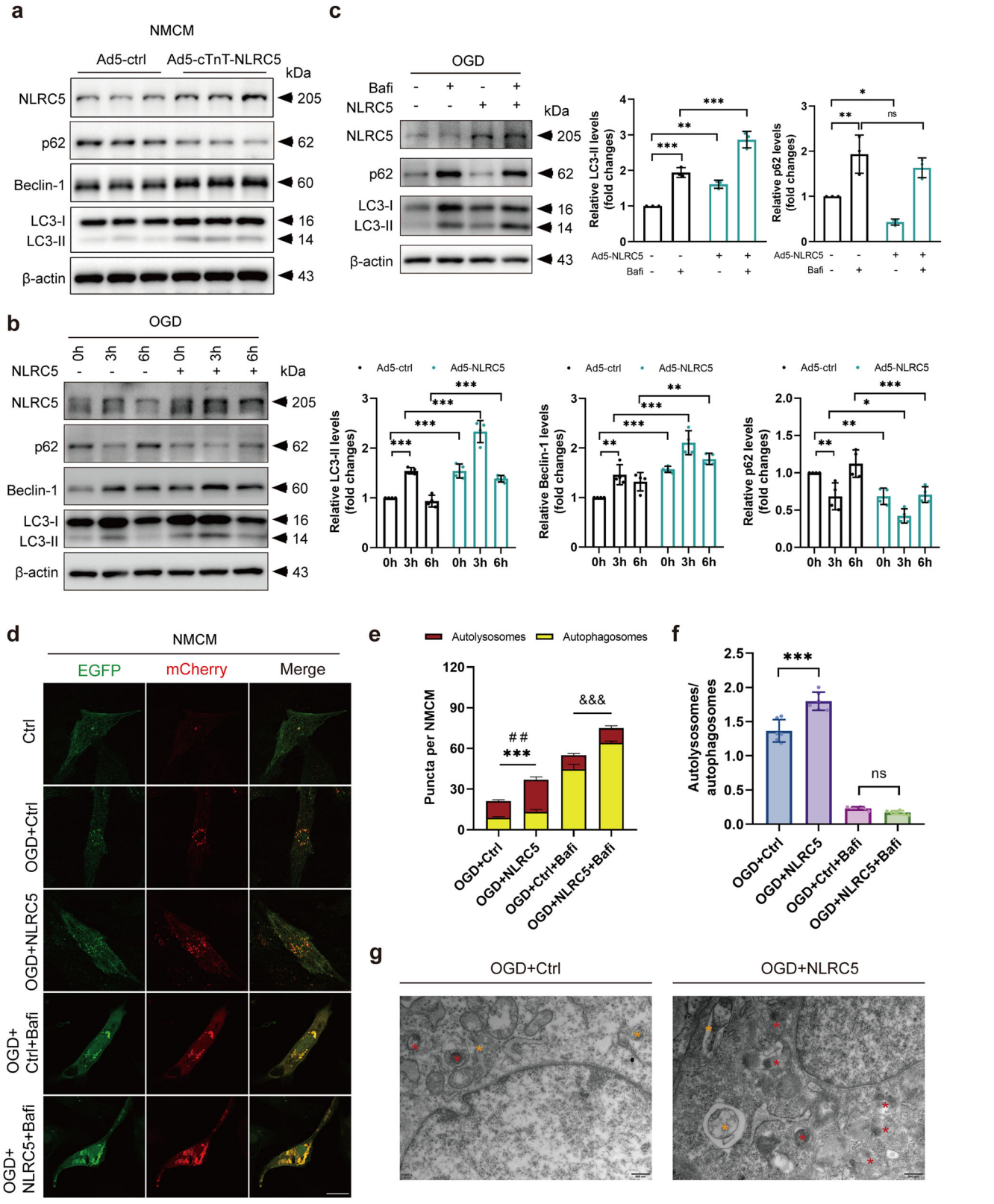

is known to be a key site for ubiquitination and mediates the degradation of CAVIN1 through proteasomal pathways[44]. These findings suggest that NLRC5 may facilitate the degradation of CAVIN1 via interaction with its HR1 domain. Additionally, CAVIN1 knockdown in NMCMs significantly enhanced autophagy, counteracting the inhibitory effects of NLRC5 knockdown on autophagic flux.

This study demonstrated that NLRC5 overexpression led to a reduction in the expression of the CAVIN1-associated protein, CAV1. Recent studies have identified CAV1 as a negative regulator of autophagy activation in various cell types, including adipocytes, cancer cells, and endothelial cells[45–48]. In NMCMs, CAV1 downregulation promoted autophagic activity, which was associated with an increased expression of ATG12-ATG5

Fig. 3 | NLRC5 overexpression promotes autophagy flux in NMCMs under OGD stimulation. a NLRC5, p62, Beclin-1, and LC3-II proteins were detected by Western blot in NMCMs transfected with Ad5-Ctrl or Ad5-cTnT-NLRC5 (multiplicity of infection [MOI], 100) ($n = 3$ each). **b** Representative western blot of NLRC5, p62, Beclin-1, and LC3-II in NMCMs transfected with Ad5-Ctrl or Ad5-cTnT-NLRC5 followed by 0, 3, 6 h of OGD and corresponding quantification ($n = 4$ each). **c** NMCMs were transfected with Ad5-Ctrl or Ad5-cTnT-NLRC5 and then treated with or without bafilomycin A1 (100 nM) to evaluate autophagic flux under OGD for 6 h. Representative western blot of LC3-II and p62 and corresponding quantification ($n = 3$ each). **d** Representative immunofluorescence images demonstrating NMCMs co-transfected with Ad5-Ctrl or Ad5-cTnT-NLRC5 and an adenovirus over-expressing mCherry-EGFP-LC3 for 48 h in the presence or absence of bafilomycin A1 or OGD to evaluate LC3 puncta. Yellow dots (merged red and green) indicate autophagosomes whereas red-only dots indicate autolysosomes. Representative of $n = 6$ experiments. Scale bar, 20 μm. **e, f** Quantitative analysis of autophagosomes, autolysosomes, and ratio of autolysosomes to autophagosomes in NMCMs treated as in **d** from six independent experiments. **g** Representative transmission electron microscopy (TEM) images of autophagosomes and autolysosomes structure in NMCMs transfected with Ad5-Ctrl or Ad5-cTNT-NLRC5 under OGD. Asterisks represent autophagosomes (yellow) and autolysosomes (red). Scale bar, 500 nm. Data are presented as mean ± SD. **b, c, e** 2-way ANOVA with Sidak multiple comparisons test. **f** 1-way ANOVA with Tukey multiple comparisons test. $^{*}P < 0.05$, $^{**}P < 0.01$, and $^{***}P < 0.001$. **e** $^{***}P < 0.001$, comparison between red dots, $^{\#\#}P < 0.01$, comparison between yellow dots, and $^{\&\&\&}P < 0.001$, comparison between total of red and yellow dots. ns indicates not significant.

proteins. To investigate whether NLRC5-mediated degradation of CAVIN1 resulted in a concomitant decrease in CAV1 levels, thereby facilitating autophagy, the effects of CAV1 overexpression were examined in the context of NLRC5 overexpression. The results indicated that CAV1 overexpression suppressed autophagy and negated the cardioprotective effects induced by NLRC5 overexpression in MI mice, highlighting that CAV1 plays a pivotal role in modulating cardiomyocyte autophagy following NLRC5 activation. These findings reinforce the hypothesis that NLRC5 exerts a protective effect on the ischemic heart by enhancing cardiomyocyte autophagy through its interaction with CAVIN1 and the subsequent downregulation of CAV1.

While the current study provides compelling evidence for the cardioprotective role of NLRC5 in MI, several limitations warrant consideration. A notable challenge is that the molecular weight of NLRC5 exceeds the size limit for adeno-associated virus (AAV) constructs, which restricts the exploration of NLRC5's long-term effects in the post-MI setting. Additionally, NLRC5 has only been tested in the MI mouse model, and its efficacy in alleviating ischemia/reperfusion (I/R) injury remains unexplored, necessitating further investigation. Finally, while trichrome staining of representative sections provides valuable insights into regional fibrotic changes, it does not allow for precise quantification of total scar size in the entire heart. Future studies could employ methods such as hydroxyproline assays or late gadolinium enhancement MRI for a more comprehensive evaluation of fibrosis and scar formation.

In conclusion, this study identifies NLRC5 as a pivotal regulator of cardiomyocyte autophagy in MI. Targeting the NLRC5–CAVIN1–CAV1 signaling axis could thus provide a promising therapeutic strategy for the treatment of MI.

Materials and methods

Animal

All animal experiments were conducted in accordance with the guidelines established by the National Institutes of Health (NIH) in the publication "Guide for the Care and Use of Laboratory Animals" (2011). Ethical approval was obtained from the Animal Management and Use Committee and the Animal Ethics Committee of Nanjing Medical University (Approval No. 2403035). In this study, eight-week-old male Institute of Cancer Research (ICR) mice were sourced from the Animal Core Facility of Nanjing Medical University (Nanjing, China). The mice were housed in a standard pathogen-free (SPF) environment at the Laboratory Animal Center of Nanjing Medical University, with a 12:12 light-dark cycle, temperature maintained at 20–22 °C, and relative humidity set between 50% and 70%. Ad libitum access to food and water was provided throughout the duration of the study.

Recombinant adenovirus, plasmids and siRNAs

Recombinant adenoviruses used in this study were procured from commercial suppliers. Genechem (Shanghai, China) provided Ad5-cTnT-NLRC5, an adenovirus encoding mouse *Nlrc5* mRNA under the control of a cardiomyocyte-targeted cardiac troponin T promoter. Ad5-cTnT-Ctrl served as the control adenovirus. Additionally, Genechem supplied Ad5-cTnT-NLRC5i, which contains shRNA sequences targeting mouse *Nlrc5*, and Ad5-cTnT-Ctrli, a control adenovirus with scrambled shRNA sequences. The specific target sequence for the shRNA against mouse *Nlrc5* was 5′-ATAGTAGGCAAACTCCTGCAG-3′. HanBio (Shanghai, China) provided Ad5-cTnT-CAV1, which encodes mouse *Cav1* mRNA, as well as Ad5-cTnT-Ctrl as the control adenovirus, and tandem mCherry-EGFP-LC3 adenoviral vectors. Plasmids encoding Flag-NLRC5, Flag-CARD, Flag-NACHT, Flag-LRR, HA-CAVIN1, HA-HR1, and HA-HR2 were obtained from Genechem (Shanghai, China). For the siRNA experiments, RiboBio (Guangzhou, China) supplied siRNAs targeting mouse *Nlrc5*, *Cavin1*, and *Cav1*. The specific target sequences for the siRNAs were 5′-AGGCTGGACTTCTCCATCA-3′ for mouse *Nlrc5*, 5′-GCTGAGCCTTCTGGATAAA-3′ for mouse *Cavin1*, and 5′-GCAA-GAUAUUCAGCAACAUTT-3′ for mouse *Cav1*.

Mouse MI model

The MI model in each single adult mice was induced surgically, as previously described[49]. Mice were anesthetized intraperitoneally with 1.2% Avertin (Sigma-Aldrich, Missouri, USA) and subsequently mechanically ventilated following tracheal intubation. The chest cavity was accessed via a careful dissection of the intercostal muscles, and the left anterior descending (LAD) artery was ligated using a 7-0 silk suture. Successful ligation was confirmed by the color change at the apex observed visually. A microsyringe with a 36-gauge needle was utilized to inject adenovirus into the hearts of postnatal day 56 (P56) mice. The viral dose was 2.5×10^8 pfu per mouse, diluted in a 10% trypan blue solution in phosphate-buffered saline (PBS). The needle was inserted into the ventricular myocardium, and the adenovirus was injected into the peri-infarct region, defined as the boundary between the infarcted and non-infarcted myocardium, at three distinct locations in a circular pattern. Following injection, the chest was closed using a 6-0 silk suture, and the skin was sealed with 3-0 silk sutures. Sham-operated controls underwent identical procedures without coronary occlusion. Post-operative monitoring continued until mice regained consciousness in a warm cage. Echocardiographic examinations were conducted one day post-injection, and mice with EF between 40% and 60% were selected for further analysis. The surgeon performing the procedure was blinded to the group assignment and treatment.

Echocardiography

All echocardiographic assessments were performed at the Animal Laboratory Center of Nanjing Medical University. Mice were anesthetized with 0.5–1.0% isoflurane during imaging. Cardiac function was evaluated using a 40-MHz mouse ultrasound probe (VisualSonics Vevo 2100, VisualSonics, Toronto, Canada). Parameters assessed included LVID; d, LVID; s, left ventricular end-systolic volume (LVESV), and left ventricular end-diastolic volume (LVEDV). Cardiac function was quantified by calculating the EF (EF = ([LVEDV-LVESV]×100/LVEDV)) and fractional shortening (FS = [LVID; d-LVID; s] × 100/LVID; d). Heart rate was continuously monitored during the procedure. Raw echocardiographic data are presented in Supplementary Tables 1–4.

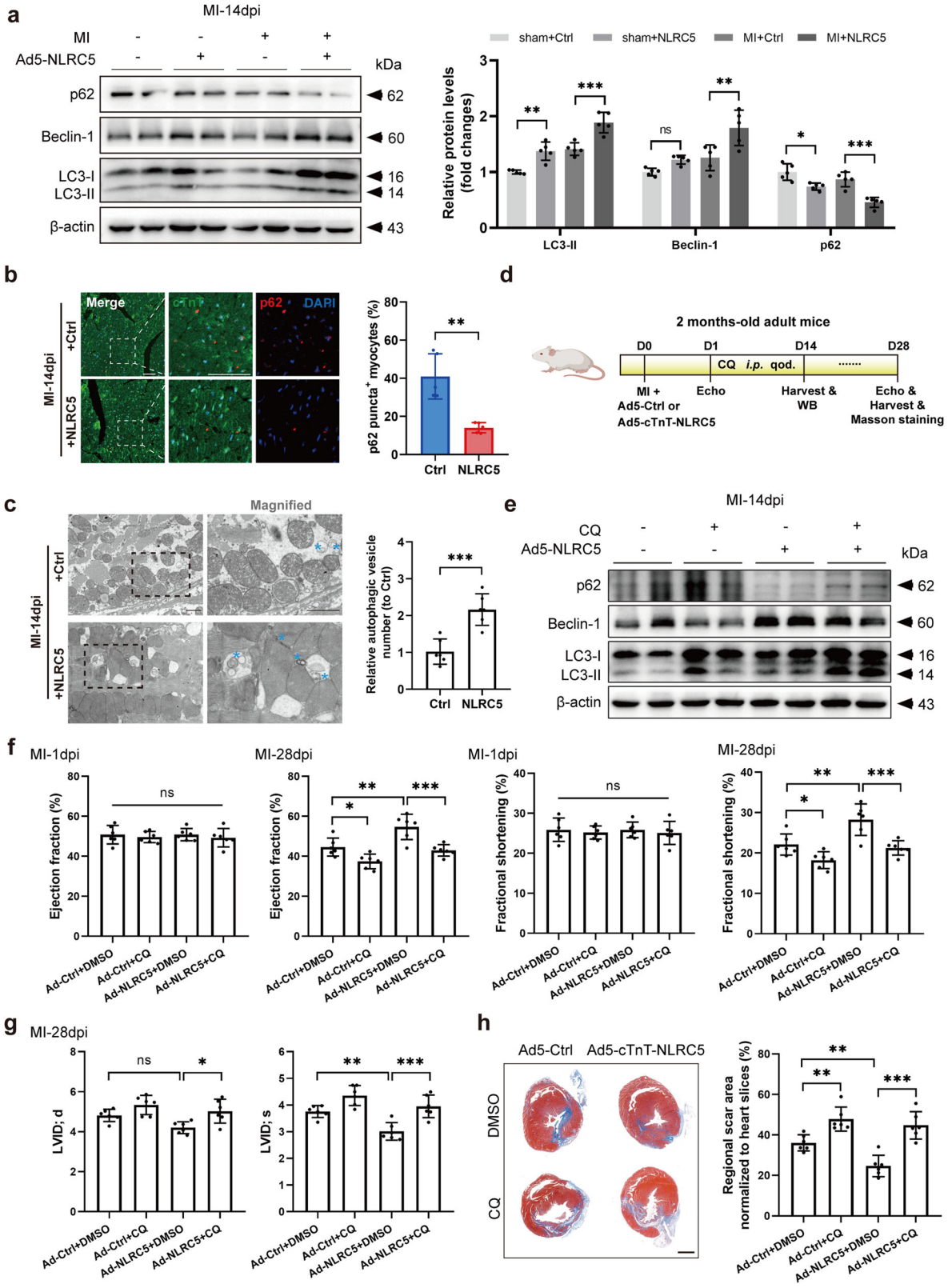

Study protocols

For the MI mouse model, the comparison of MI surgery was conducted on the following groups: (1) P56 mice injected with Ad5-cTnT-Ctrli (control) and Ad5-cTnT-NLRC5i in Fig. 1; (2) P56 mice injected with Ad5-cTnT-Ctrl (control) and Ad5-cTnT-NLRC5 in Fig. 2; (3) P56 mice injected with Ad5-cTnT-Ctrl + DMSO (control), Ad5-cTnT-Ctrl + CQ, Ad5-cTnT-NLRC5 + DMSO, and Ad5-cTnT-NLRC5 + CQ in Fig. 4; (4) P56 mice injected with Ad5-cTnT-Ctrl (control), Ad5-cTnT-NLRC5, Ad5-cTnT-CAV1, Ad5-cTnT-NLRC5 + Ad5-cTnT-CAV1 in Fig. 7. All adenoviruses were administered at an equal titer of 2.5×10^8 pfu/mouse, diluted in a 10% trypan blue solution in PBS, and directly injected into the peri-infarct myocardium of P56 mice immediately following MI induction. Injection

Fig. 4 | NLRC5 overexpression protects ischemic myocardium and improves the cardiac function through enhancing autophagy in mice post MI. a p62, Beclin-1 and LC3-II proteins were detected by Western blot in hearts transfected with Ad5-Ctrl or Ad5-cTnT-NLRC5 at 14 days post-MI (dpi) ($n = 5$ each). **b** Immunofluorescence staining of p62 in heart tissues transfected with Ad5-Ctrl or Ad5-cTnT-NLRC5 at 14 dpi and corresponding quantification ($n = 5$ hearts for each group). Scale bar, 20 μm. **c** Transmission electron microscopy images and corresponding quantification of autophagic vesicles in myocardium transfected with Ad5-Ctrl or Ad5-cTnT-NLRC5 at 14 dpi. Asterisks (blue) represent autophagic vesicles ($n = 6$ hearts for each group). Scale bar, 1 μm. **d** The experimental timeline for the MI model. Ad5-Ctrl or Ad5-cTnT-NLRC5 were injected to peri-infarct myocardium of adult mice during MI surgery. Chloroquine (CQ, 10 mg/kg) or diluted DMSO was administered via intraperitoneal injection (i.p.) for four weeks at two days interval. Echocardiographic analyses were performed at 1 and 28 dpi. Hearts were harvested at 14 and 28 dpi for histological analyses. **e** Representative Western blots showing expression of p62, Beclin-1, and LC3-II for autophagy proteins in hearts transfected with Ad5-Ctrl or Ad5-cTnT-NLRC5 in the presence or absence of CQ treatment at 14 dpi ($n = 4$ each). **f, g** Quantitative analysis of LVEF, LVFS, LVID; d, and LVID; s in mice treated with Ad5-Ctrl or Ad5-cTnT-NLRC5 in the presence or absence of CQ treatment at 28 and/or 1 dpi ($n = 6$ per group). **h** Masson staining and corresponding quantification of regional scar area in hearts of mice treated with Ad5-Ctrl or Ad5-cTnT-NLRC5 in the presence or absence of CQ treatment at 28 dpi ($n = 6$ each). Scale bar, 1 mm. Data are presented as mean ± SD. **b, c** Standard unpaired Student *t* test. **a, f-h**, 1-way ANOVA with Tukey multiple comparisons test. $^{*}P < 0.05$, $^{**}P < 0.01$, and $^{***}P < 0.001$. ns indicates not significant.

was performed using a 36-gauge needle mounted on a microsyringe. Mice exhibiting successful MI models, defined by echocardiographic confirmation (EF% between 40% and 60% at 1 dpi), were further monitored and euthanized via CO_2 inhalation at the specified time points. NLRC5 expression within the infarct border zone and sham tissue was assessed by WB and IF staining. Inflammatory markers (*Il-6*, *Tnf-α* mRNA) and fibrotic markers (*Col1a1*, *Col3a1*, and *Mmp2*) mRNA levels were quantified by quantitative RT-PCR at the indicated time points. Cardiac function was evaluated by serial echocardiography at 1, 7, 14, and 28 dpi. Infarcted areas were assessed at 7 dpi using TTC staining, and regional scar area was evaluated at 28 dpi using Masson trichrome staining.

To investigate the effects of NLRC5 on myocardial autophagy and autophagic flux, markers of autophagy (p62, Beclin-1, LC3-II/I) in the border zone were evaluated by WB and IF. Autophagic vesicles in the border zone were visualized via TEM. Additionally, autophagy was inhibited by administering CQ (10 mg/kg intraperitoneally) or diluted DMSO one day after MI, with treatments given every two days for four weeks. CQ, a known autophagy inhibitor, prevents the fusion of autophagosomes with lysosomes. The selected dosage of CQ has been validated in previous studies to effectively suppress autophagy without significant adverse effects on cardiac tissue[50,51].

To explore the functional downstream signaling of NLRC5, the CAVIN1/CAV1 axis was targeted for interference. NMCMs were treated with siRNAs targeting CAVIN1 and/or NLRC5 or CAV1. In vivo, Ad5-cTnT-CAV1 and/or Ad5-cTnT-NLRC5 were injected into the peri-infarct myocardium of P56 mice following MI induction. There was no statistical method for pre-determining sample size. Mice were randomly assigned to treatment groups using an online random number generator. The surgeon performing the procedures was blinded to the group allocation, and all subsequent analyses were conducted by researchers blinded to the experimental conditions. No data was excluded. Only male mice were utilized in these in vivo studies, given the conflicting evidence regarding the role of estrogen in MI. Estrogen has been shown to potentially exacerbate MI during acute events, while also suggesting benefits for long-term survival[52,53], warranting the use of male mice to minimize hormonal confounding factors.

Myocardium collection in infarct border zone

At indicated time post infarction, the mice were euthanized by CO_2 inhalation. The heart was rapidly separated and the blood was thoroughly rinsed in pre-cooled PBS. Then the myocardium in infarct border zone was carefully separated. The infarct border zone was defined as the myocardial tissue located at a distance of 1-2 mm from the edge of the infarction.

TTC staining and assessment of infarct size

At 7 days post-infarction, infarcted myocardial size was quantified using Evans blue/TTC staining. Briefly, hearts were perfused with saline via a Langendorff system to remove blood, followed by staining with a 1% Evans blue solution and subsequent incubation in a 1% TTC-Tris solution at 37 °C for 15 min. The infarcted area (white) was measured relative to the total left ventricular area using ImageJ software.

Masson trichrome staining and assessment of local collagen deposition

Regional scar area at 28 dpi was assessed by Masson trichrome staining, where the collagen deposition area (blue) was quantified relative to the representative cross-sectional area of the heart slices. Transverse heart sections from the apex to the base were collected, and measurements from at least six mice per group were performed at each level, with analyses conducted using ImageJ software. All measurements were carried out in a blinded manner to ensure objectivity.

Cell culture and intervention

NMCMs were isolated from the hearts of 1-day-old neonatal ICR mice following established protocols[54]. In brief, hearts from P0 mice were minced, followed by digestion with a mixture containing 0.6 mg/ml pancreatin (Sigma-Aldrich) and 0.4 mg/ml collagenase type 2 (Worthington, Colorado, USA). After filtration through a 40-μm strainer, the cells were plated and cultured in Dulbecco's modified Eagle's medium (DMEM; Thermo Fisher Scientific/Gibco, Massachusetts, USA) supplemented with 10% fetal bovine serum (FBS; Gibco) and 1% Penicillin-Streptomycin (P/S; Gibco) at 37 °C for 1 h to allow fibroblast adhesion. Non-adherent cells were separated using Percoll gradient centrifugation (Cytiva, Massachusetts, USA) for further purification of NMCMs. Enriched cardiomyocytes were plated on gelatin-coated (Sigma-Aldrich) dishes and cultured in DMEM supplemented with 10% horse serum (HS; Gibco), 5% FBS, and 1% P/S. After 24 h, the non-adherent cells were removed by washing, and the remaining cells were cultured for an additional 12 h before being treated with adenovirus, siRNAs, or specific reagents.

The HEK-293T cell line (batch number: 230330F101), and AC16 cell line (batch number: 240531X201) were obtained from Haixing Bioscience (Suzhou, China). Species verification of the cell lines was performed through cytochrome B PCR followed by Sanger sequencing. Prior to experimentation, the absence of Mycoplasma contamination was confirmed, and the cells were cultured in DMEM supplemented with 10% FBS. After 24 h of culture, HEK-293T cells were transfected with NLRC5 and CAVIN1 full-length or truncated plasmids using Lipofectamine 3000 according to the manufacturer's protocol. The cell lines used in the experiments were cultured for a maximum of 20 passages. To induce OGD, cells were incubated with glucose- and serum-free DMEM in a 2.5L sealable jar, using MGC AnaeroPACK (Mitsubishi Gas Chemical Company, Tokyo, Japan). OGD conditions were maintained at 37 °C with a gas composition of 95% N_2 and 5% CO_2 for the specified duration.

Immunoblotting and antibodies

Heart tissues or cells were lysed using Whole Cell Lysis Buffer (Cat Number: KGB5303-100, Keygen Biotech, Nanjing, China) supplemented with protease and phosphatase inhibitor cocktail (Selleck, Texas, USA). The lysates were centrifuged at 18,800 RCF (g-force) for 20 min at 4 °C, and the supernatant was collected. To prepare the samples for WB analysis, the

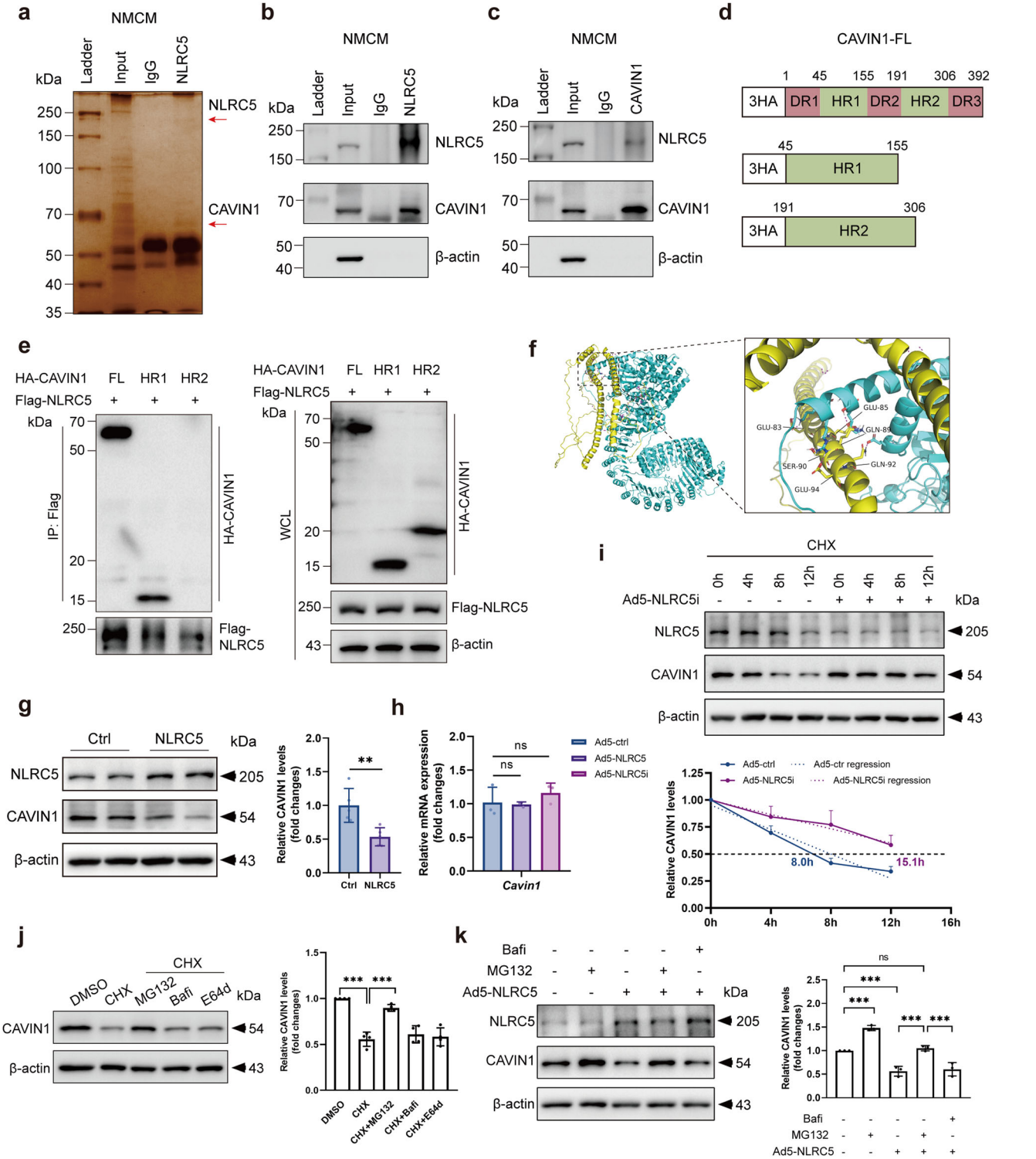

Fig. 5 | NLRC5 interacts with CAVIN1 and regulates its stability. **a** Immunoprecipitation of NLRC5 binding partners. NLRC5 was overexpressed in neonatal mouse cardiomyocytes (NMCMs) through Ad5-cTnT-NLRC5. The cell lysate was immunoprecipitated using either IgG (control) or anti-NLRC5 antibody. Immunoprecipitated samples were subjected to SDS-PAGE followed by silver staining. Co-immunoprecipitation (Co-IP) assays assessed the interaction between NLRC5 and CAVIN1 in both anti-NLRC5 pull-down NMCM samples (**b**) and anti-CAVIN1 pull-down NMCM samples (**c**). Input was used as positive controls and anti-IgG pull-down samples were assessed as negative controls. **d** Illustration of the truncated domains of CAVIN1. **e** Co-IP of HEK-293T cells overexpressing Flag-NLRC5 and HA-tagged CAVIN1 or truncated forms followed by Western blot. **f** Molecular docking analysis of the NLRC5 and CAVIN1 domains, with CAVIN1 in yellow and NLRC5 in cyan. **g** Expression of CAVIN1 and NLRC5 in NMCMs 48 h after transfected with Ad5-Ctrl or Ad5-cTnT-NLRC5 ($n = 5$ each). **h** Quantitative RT-PCR analysis of the mRNA levels of *Cavin1* in NMCMs transfected with Ad5-Ctrl, Ad5-cTnT-NLRC5 or Ad5-cTnT-NLRC5i ($n = 3$ each). **i** Half-life of CAVIN1 protein in NMCMs treated with or without NLRC5 knockdown in the presence of 0.4mM CHX for 0, 4, 8, 12h ($n = 3$ each). **j** Western blot and corresponding quantification of CAVIN1 protein level in NMCMs treated with 0.4 mM CHX in the presence or absence of MG-132 (20 μM), bafilomycin A1 (100 nM), or E64d (10 μM) for 8 h ($n = 4$ each). **k** Western blot and corresponding quantification of CAVIN1 in NLRC5 overexpressed NMCMs with or without MG-132 (20 μM) for 8 h ($n = 3$ each). Data are presented as mean ± SD. **g** Standard unpaired Student *t* test. **h, j, k** 1-way ANOVA with Tukey multiple comparisons test. **i** Calculation using equation fitted by linear regression. $^{*}P < 0.05$, $^{**}P < 0.01$, and $^{***}P < 0.001$. ns indicates not significant.

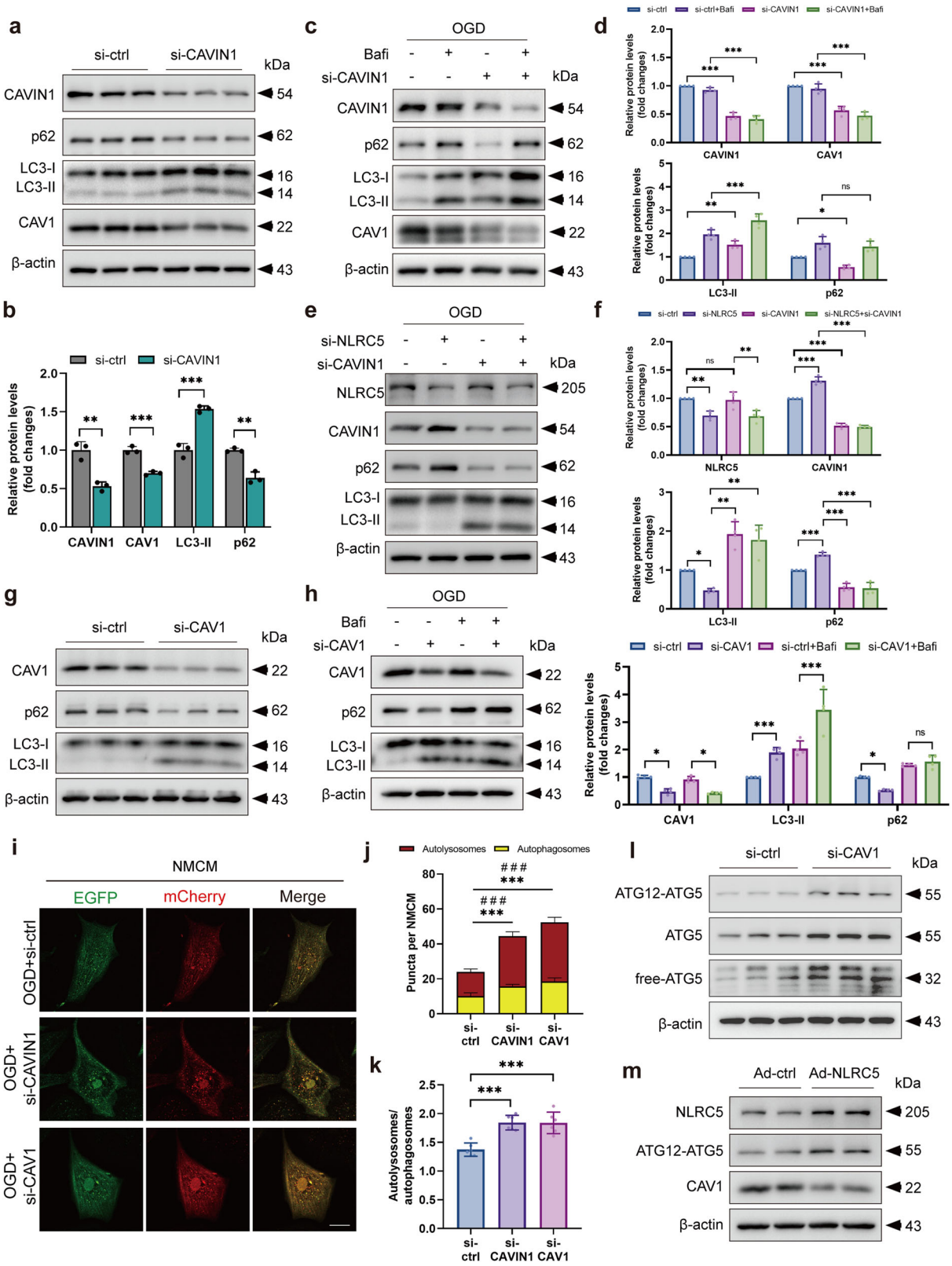

supernatant was mixed with 5 × SDS loading buffer (Fdbio, Hangzhou, China) and heated at 99 °C for 10 min. The protein samples were separated on 6–15% gradient SDS-PAGE gels (Epizyme, Shanghai, China) and then transferred onto PVDF membranes (Millipore, Massachusetts, USA) via electroblotting. The membranes were blocked with 5% skim milk in TBS-T for 2 h and incubated overnight with primary antibodies. The following primary antibodies were used: NLRC5 (ab105411) from Abcam, CAV1 (3267S), Atg12 (4180T), Atg5 (12994T), p70S6K (2708T), p-p70S6K (9234T), AMPKα (5831T), p-AMPKα (2535T), β-actin (4970S) from Cell Signaling Technology, p62/SQSTM1 (18420-1-AP), LC3B (14600-1-AP), Beclin-1 (11306-1-AP), Atg5 (10181-2-AP), AKT (60203-2-Ig), p-AKT (66444-1-Ig), CAVIN1 (18892-1-AP), CAV1 (66067-1-Ig) from Proteintech, Flag-Tag (PM020) from MBL, and HA-Tag (sc-7392) from Santa Cruz. After three washes with TBS-T, the membranes were incubated with

Fig. 6 | CAVIN1 knockdown reverses the inhibited autophagy induced by NLRC5 knockdown. a, b Western blot and corresponding quantification of CAVIN1, p62, LC3-II and CAV1 in neonatal mouse cardiomyocytes (NMCMs) treated with si-ctrl or si-CAVIN1 ($n = 3$ each). **c, d** NMCMs were transfected with si-ctrl or si-CAVIN1 and then treated with bafilomycin A1 (100 nM) to evaluate autophagic flux under oxygen-glucose deprivation (OGD) for 6 h. Representative western blot for CAVIN1, CAV1, LC3-II, p62 and corresponding quantification ($n = 4$ each). **e, f** Western blot and corresponding quantification of NLRC5, CAVIN1, p62, and LC3-II in NMCMs treated with si-ctrl, si-NLRC5, si-CAVIN1, or si-NLRC5+si-CAVIN1 followed by OGD for 6h ($n = 4$ each). **g** Western blot of CAV1, p62, and LC3-II in NMCMs treated with si-ctrl or si-CAV1 ($n = 3$ each). **h** NMCMs were transfected with si-ctrl or si-CAV1 and then treated with bafilomycin A1 (100 nM) to evaluate autophagic flux under OGD for 6 h. Representative Western blot for CAV1, LC3-II, p62 and corresponding quantification ($n = 4$ each). **i** Representative immunofluorescence images demonstrating NMCMs co-transfected with si-ctrl or si-CAVIN1 or si-CAV1 and mCherry-EGFP-LC3 adenovirus followed by OGD for 6h to evaluate LC3 puncta. Yellow dots (merged red and green) indicate autophagosomes whereas red-only dots indicate autolysosomes. Representative of $n = 6$ experiments. Scale bar, 20 μm. **j, k** Quantitative analysis of autophagosomes, autolysosomes, and ratio of autolysosomes to autophagosomes in NMCMs treated as in **g** from six independent experiments. **l** Western blot of ATG12-ATG5, ATG5, and free-ATG5 in NMCMs treated with si-ctrl or si-CAV1 ($n = 3$ each). **m** Representative Western blot of NLRC5, ATG12-ATG5, and CAV1 in NMCMs treated with Ad5-Ctrl or Ad5-cTnT-NLRC5. Data are presented as mean ± SD. **b** Standard unpaired Student *t* test. **d, h, j** 2-way ANOVA with Sidak multiple comparisons test. **f, k** 1-way ANOVA with Tukey multiple comparisons test. $^{*}P < 0.05$, $^{**}P < 0.01$, and $^{***}P < 0.001$. **j** $^{***}P < 0.001$, comparison between red dots, $^{\#\#\#}P < 0.001$, comparison between yellow dots. ns indicates not significant.

horseradish peroxidase (HRP)-labeled secondary antibody (Fdbio, 1:10,000 dilution) for 2 h at room temperature. Following washes, antibody-antigen complexes were visualized using the ChemiDoc Imaging System with Image Lab software (Bio-Rad, California, USA). ImageJ software (ImageJ, Maryland, USA) was used for brightness adjustment and quantification.

Quantitative RT-PCR

Total RNA was extracted from the tissues or cells using TRIzol reagent (Takara, Tokyo, Japan). Reverse transcription was performed using HiScript III All-in-one RT SuperMix (Vazyme, Nanjing, China). Quantitative RT-PCR was performed using the QuantStudio 5 Flex system (ABI, Foster City, USA) with SYBR Green Premix (Vazyme) for RNA quantification. *Actb* was used as the internal control. Primer sequences for quantitative RT-PCR are provided in Supplementary Table 5.

Chemicals

All chemicals used in this study are listed in Supplementary Table 6.

Co-IP, silver staining, and MS

For Co-IP assays, lysates of NMCMs or HEK-293T cells were prepared in lysis buffer supplemented with protease and phosphatase inhibitors. The lysates were incubated overnight at 4 °C with gentle rotation along with anti-NLRC5 antibody or rabbit IgG antibody. To capture the protein-antibody complexes, rProtein A/G MagPoly beads (ACE, Nanjing, China) were added and incubated for 4 h at 4 °C with gentle rotation. The bead-protein-antibody complexes were washed with elution buffer and then denatured at 99 °C for 10 min in 1 × loading buffer. The proteins were analyzed by WB and MS (OE Biotech, Shanghai, China). Silver staining of proteins was performed using the Fast Silver Stain Kit (Beyotime) according to the manufacturer's instructions. The proteins identified by MS in Co-IP experiments using anti-NLRC5 or IgG antibody in NMCMs are provided in Supplementary Data 1 and 2.

IF

For IF, infarct border sections were deparaffinized, permeabilized with 0.1% Triton X-100, and blocked with 5% BSA at room temperature for 2 h. The sections were then incubated overnight at 4 °C with primary antibodies, including anti-p62 (18420-1-AP, Proteintech), anti-NLRC5 (ab105411, Abcam), anti-CAVIN1 (M028121S, Abmart), anti-cardiac troponin T (ab8295, Abcam), anti-Vimentin (10366-1-AP, Proteintech), anti-CD68 (28058-1-AP, Proteintech), and anti-CD31 (ab24590, Abcam), all at a dilution of 1:200. After washing with PBS, the sections were incubated with Alexa Fluor 488- and 555-conjugated secondary antibodies (A-11001, A-21428, Thermo Fisher) at a dilution of 1:400 for 2 h, protected from light. Cell nuclei were counterstained with 4',6-diamidino-2-phenylindole (DAPI, Sigma-Aldrich). To evaluate the cardiomyocyte cross-sectional area, wheat germ agglutinin (WGA) staining (w32466, Thermo Fisher) was performed. Images were captured using a THUNDER Imager (Leica, Wetzlar, Germany).

TEM

Freshly collected NMCMs or heart tissues were fixed immediately in 2% glutaraldehyde in 0.1 M phosphate-buffered saline, followed by further fixation with 1% osmium tetroxide. Samples were then dehydrated using ethanol, embedded in epon resin, and cut into ultrathin sections of approximately 50 nm thickness. These sections were stained with 3% uranyl acetate and lead citrate. Stained sections were examined under a transmission electron microscope (JEM-1400 Flash, JEOL, Tokyo, Japan) at 120 kV.

Cell viability assay

NMCMs were seeded at a density of 1×10^4 cells per well in a 96-well plate. After the specified treatments, CCK-8 reagent (Dojindo, Kumamoto, Japan) was added to each well, followed by exposure of the cells to OGD. The cells were incubated for the recommended duration to allow the development of color indicative of viable cells, as a result of the reaction between the viable cells and the CCK-8 reagent. Following incubation, absorbance at 450 nm was measured using a microplate reader (Synergy 2, BioTek, Vermont, USA). Cell viability was calculated by comparing the absorbance values of the treated groups to those of the control groups under OGD conditions. This approach allows for the quantification of viable cells and provides a reliable assessment of cell death across various treatment groups.

Autophagic flux assay

For autophagy analysis, NMCMs were seeded in confocal dishes and transfected with mCherry-EGFP-LC3 adenoviral vectors. After treatment, LC3 puncta were visualized using a fluorescence confocal microscope (Stellaris STED, Leica).

Molecular docking analysis

To investigate the structure and interaction of NLRC5 and CAVIN1, the protein structure of NLRC5 and CAVIN1 was retrieved from the AlphaFold Protein Structure Database (https://alphafold.ebi.ac.uk/; last updated on 2022-11-01, using the AlphaFold Monomer v2.0 pipeline). The binding mode of NLRC5 and CAVIN1 was predicted using the 'ClusPro 2.0' server[55]. The optimal structure was determined by selecting the cluster with the largest size, corresponding to the highest number of docked structures rather than energy, based on the balanced coefficients recommended by ClusPro[56]. This method allowed the identification of the most representative binding conformation of the NLRC5-CAVIN1 complex.

RNA sequencing analysis

The RNA-seq dataset detailing time-series gene expression in murine heart tissue following MI was obtained from the Gene Expression Omnibus (GEO) (GSE206281, https://www.ncbi.nlm.nih.gov/geo/query/acc.cgi?acc=GSE206281). Gene counts derived from this dataset were analyzed to explore the relationship between NLRC5 and autophagy markers, using control (CTRL), 1dpi, and 3dpi data. Correlation plots were generated with the ggstatsplot package, and the Spearman correlation coefficient was

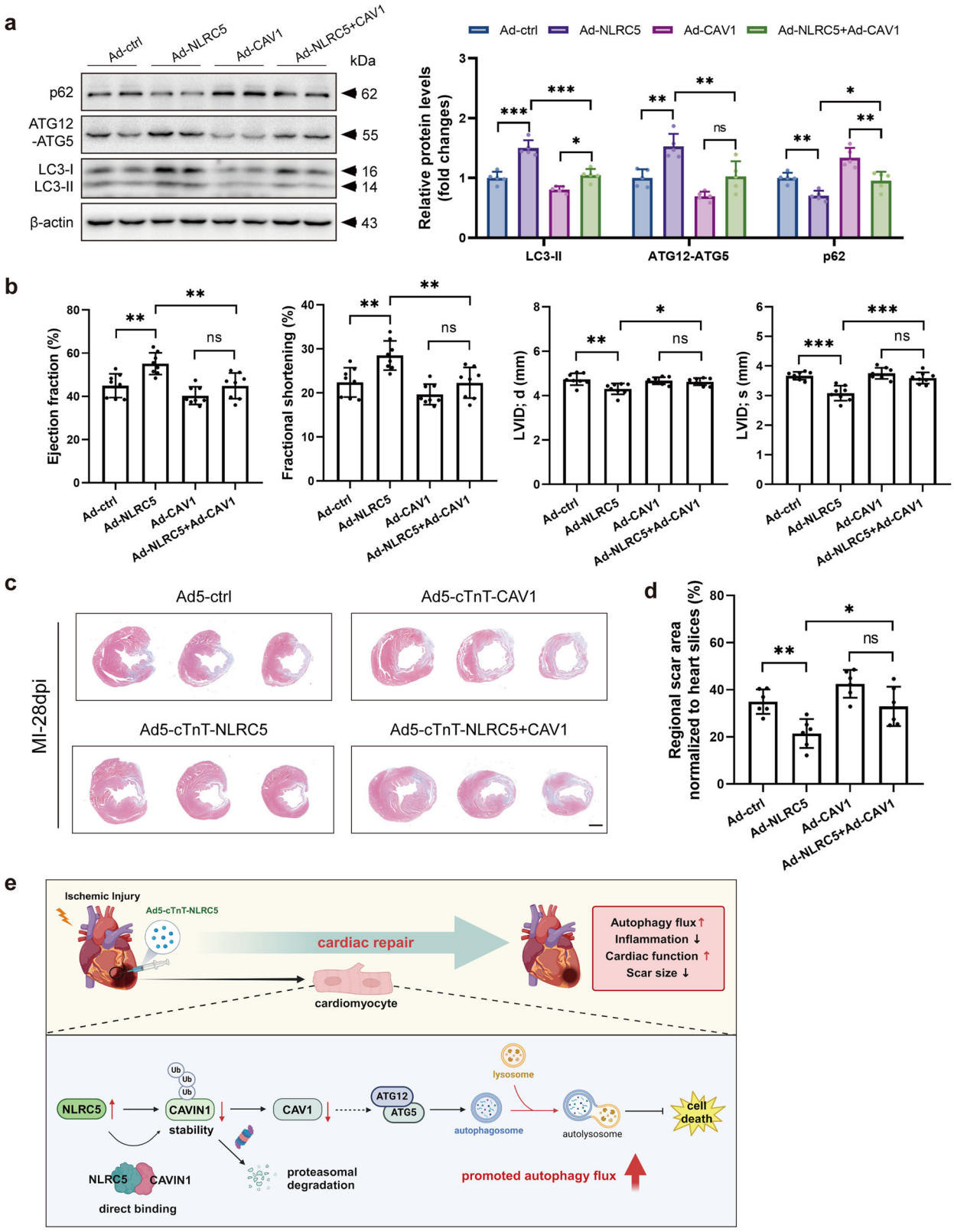

Fig. 7 | CAV1 overexpression attenuates the cardioprotective effects of NLRC5 overexpression in mice post MI. a Representative Western blots and corresponding quantification of p62, ATG12-ATG5, and LC3-II for autophagy proteins in hearts transfected with Ad5-Ctrl, Ad5-cTnT-NLRC5, Ad5-cTnT-CAV1, or Ad5-cTnT-NLRC5 + CAV1 at 14 days post-MI (dpi) ($n = 5$ each). **b** Quantitative analysis of LVEF, LVFS, LVID; d, and LVID; s in mice treated with Ad5-Ctrl, Ad5-cTnT-NLRC5, Ad5-cTnT-CAV1, or Ad5-cTnT-NLRC5 + CAV1 at 28 dpi ($n = 8$ per group). **c, d** Regional scar area and corresponding quantification in Ad5-Ctrl, Ad5-cTnT-NLRC5, Ad5-cTnT-CAV1, or Ad5-cTnT-NLRC5 + CAV1 hearts shown by Masson trichrome staining of heart tissue sections at 28 dpi ($n = 6$ each). Scale bar, 1 mm. **e** Schematic model of NLRC5 exerting cardioprotective effect by promoting CAVIN1/CAV1-mediated autophagy (figure drawn using BioRender). Data are presented as mean ± SD. **a, b, d**, 1-way ANOVA with Tukey multiple comparisons test. $^{*}P < 0.05$, $^{**}P < 0.01$, and $^{***}P < 0.001$. ns indicates not significant.

calculated to determine statistical significance. Parameters were deemed correlated when $P < 0.05$.

Single-cell RNA sequencing analysis

Single-cell nuclei RNA sequencing data from human myocardial tissue were sourced from Cellxgene, as previously described (https://cellxgene.cziscience.com/collections/8191c283-0816-424b-9b61-c3e1d6258a77)[20]. Analysis was conducted using Seurat (version 4.4.0). Data were initially loaded into Seurat objects via the Read10X function, and specific marker genes were used to identify cardiomyocytes (MYH6), fibroblasts (PDGFRA), endothelial cells (PECAM1), and myeloid cells (C1QA)[20]. To mitigate data sparsity and improve analytical robustness, particularly for large-scale datasets, the Metacell-2 method was applied[57]. This approach facilitated the transformation of sparse single-cell RNA-seq data into quantitative metacell models. The analysis focused on NLRC5 expression under three conditions: control (CTRL), infarct zone and border zone (IZ + BZ), and remote zone (RZ). Expression levels of NLRC5 were computed for each cell type across these conditions. Potential variations in NLRC5 expression between conditions and cell types were assessed using group-wise Mann-Whitney *U* tests, with results visualized in boxplots. Variable names and adjustments were tailored to accommodate the specific characteristics of the dataset and experimental design.

Statistics and reproducibility

Data are presented as mean ± SD, with the biological replicate number (n) indicated in each figure legend. Statistical analyses were performed using appropriate methods. The Shapiro-Wilk test was applied to evaluate data normality. For normally distributed datasets, comparisons between two groups utilized an unpaired Student's *t*-test, while comparisons involving more than two groups were analyzed using one-way ANOVA followed by Tukey's multiple comparison test. Two-way ANOVA with Sidak post hoc testing was used for comparisons involving multiple factors. For non-normally distributed data, the Mann-Whitney *U* test was employed. All statistical analyses were conducted in GraphPad Prism 8 (GraphPad Software), and a P value < 0.05 was considered statistically significant.

Reporting summary

Further information on research design is available in the Nature Portfolio Reporting Summary linked to this article.

Data availability

The authors declare that the data supporting the findings of this study are available within the paper and its Supplementary Information files. The numerical source data can be found in Supplementary Data 3. All relevant data are available from the authors upon request. The mass spectrometry proteomics raw data have been deposited to the ProteomeXchange Consortium via the PRIDE partner repository with the dataset identifier PXD051371.

Received: 11 April 2024; Accepted: 17 February 2025;
Published online: 23 February 2025

References

1. Tsao, C. W. et al. Heart Disease and Stroke Statistics-2023 Update: A Report From the American Heart Association. *Circulation* **147**, e93–e621 (2023).
2. Re, D. P. D., Amgalan, D., Linkermann, A., Liu, Q. & Kitsis, R. N. Fundamental Mechanisms of Regulated Cell Death and Implications for Heart Disease. *Physiol. Rev.* **99**, 1765 (2019).
3. Frangogiannis, N. G. Pathophysiology of Myocardial Infarction. In Comprehensive Physiology (ed. Terjung, R.) 1841–1875 (Wiley, 2015).
4. Moe, G. W. & Marín-García, J. Role of cell death in the progression of heart failure. *Heart Fail. Rev.* **21**, 157–167 (2016).
5. Levine, B. & Kroemer, G. Autophagy in the pathogenesis of disease. *Cell* **132**, 27–42 (2008).
6. Kaludercic, N. et al. Comprehensive autophagy evaluation in cardiac disease models. *Cardiovasc. Res.* **116**, 483–504 (2020).
7. Wang, X., Guo, Z., Ding, Z. & Mehta, J. L. Inflammation, Autophagy, and Apoptosis After Myocardial Infarction. *J. Am. Heart Assoc.* **7**, e008024 (2018).
8. Kanamori, H. et al. The role of autophagy emerging in postinfarction cardiac remodelling. *Cardiovasc. Res.* **91**, 330–339 (2011).
9. Kanamori, H. et al. Autophagy limits acute myocardial infarction induced by permanent coronary artery occlusion. *Am. J. Physiol. Heart Circ. Physiol* **300**, H2261–H2271 (2011).
10. Sciarretta, S. et al. Trehalose-Induced Activation of Autophagy Improves Cardiac Remodeling After Myocardial Infarction. *J. Am. Coll. Cardiol.* **71**, 1999–2010 (2018).
11. Sciarretta, S. et al. Activation of Nox4 in the Endoplasmic Reticulum Promotes Cardiomyocyte Autophagy and Survival during Energy Stress through the PERK/eIF-2α/ATF4 pathway. *Circ. Res.* **113**, 1253–1264 (2013).
12. Ruozi, G. et al. Cardioprotective factors against myocardial infarction selected in vivo from an AAV secretome library. *Sci. Transl. Med.* **14**, eabo0699 (2022).
13. Maejima, Y. et al. Mst1 inhibits autophagy by promoting the interaction between Beclin1 and Bcl-2. *Nat. Med.* **19**, 1478–1488 (2013).
14. Chou, W.-C., Jha, S., Linhoff, M. W. & Ting, J. P.-Y. The NLR gene family: from discovery to present day. *Nat. Rev. Immunol.* **23**, 635–654 (2023).
15. Yao, Y. et al. NLRC5 regulates MHC class I antigen presentation in host defense against intracellular pathogens. *Cell Res.* **22**, 836–847 (2012).
16. Cui, J. et al. NLRC5 Negatively Regulates the NF-κB and Type I Interferon Signaling Pathways. *Cell* **141**, 483–496 (2010).
17. He, R. et al. NLRC5 Inhibits Inflammation of Secretory Phase Ectopic Endometrial Stromal Cells by Up-Regulating Autophagy in Ovarian Endometriosis. *Front. Pharmacol.* **11**, 1281 (2020).
18. Hao, J. et al. NLRC5 restricts dengue virus infection by promoting the autophagic degradation of viral NS3 through E3 ligase CUL2 (cullin 2). *Autophagy* **19**, 1332–1347 (2023).
19. Wu, Y., Huang, C., Shi, T. & Li, J. Deficiency of NLR family member NLRC5 alleviates alcohol induced hepatic injury and steatosis by enhancing autophagy of hepatocytes. *Toxicol. Appl. Pharmacol.* **461**, 116406 (2023).
20. Kuppe, C. et al. Spatial multi-omic map of human myocardial infarction. *Nature* **608**, 766–777 (2022).
21. Li, L. et al. The role of G protein-coupled receptor kinase 4 in cardiomyocyte injury after myocardial infarction. *Eur. Heart J.* **42**, 1415–1430 (2021).
22. Mauvezin, C. & Neufeld, T. P. Bafilomycin A1 disrupts autophagic flux by inhibiting both V-ATPase-dependent acidification and Ca-P60A/SERCA-dependent autophagosome-lysosome fusion. *Autophagy* **11**, 1437–1438 (2015).
23. Schneider-Poetsch, T. et al. Inhibition of eukaryotic translation elongation by cycloheximide and lactimidomycin. *Nat. Chem. Biol.* **6**, 209–217 (2010).
24. Bai, X. et al. CAV1-CAVIN1-LC3B-mediated autophagy regulates high glucose-stimulated LDL transcytosis. *Autophagy* **16**, 1111–1129 (2020).
25. Salle-Teyssières, L. et al. Maladaptative Autophagy Impairs Adipose Function in Congenital Generalized Lipodystrophy due to Cavin-1 Deficiency. *J. Clin. Endocrinol. Metab.* **101**, 2892–2904 (2016).
26. Dávalos, A. et al. Quantitative proteomics of caveolin-1-regulated proteins: characterization of polymerase i and transcript release factor/CAVIN-1 IN endothelial cells. *Mol. Cell. Proteomics* **9**, 2109–2124 (2010).

27. Chen, Z.-H. et al. Interaction of caveolin-1 with ATG12-ATG5 system suppresses autophagy in lung epithelial cells. *Am. J. Physiol.-Lung Cell. Mol. Physiol.* **306**, L1016–L1025 (2014).
28. Chen, Z., Ding, T. & Ma, C.-G. Dexmedetomidine (DEX) protects against hepatic ischemia/reperfusion (I/R) injury by suppressing inflammation and oxidative stress in NLRC5 deficient mice. *Biochem. Biophys. Res. Commun.* **493**, 1143–1150 (2017).
29. Li, Q. et al. NLRC5 deficiency protects against acute kidney injury in mice by mediating carcinoembryonic antigen-related cell adhesion molecule 1 signaling. *Kidney Int.* **94**, 551–566 (2018).
30. Yu, Q. et al. Macrophage-Specific NLRC5 Protects From Cardiac Remodeling Through Interaction With HSPA8. *JACC Basic Transl. Sci.* **8**, 479–496 (2023).
31. Zhou, H., Yu, X. & Zhou, G. NLRC5 silencing ameliorates cardiac fibrosis by inhibiting the TGF-β1/Smad3 signaling pathway. *Mol. Med. Rep.* **16**, 3551–3556 (2017).
32. Wang, B. et al. NLRC5 deficiency ameliorates cardiac fibrosis in diabetic cardiomyopathy by regulating EndMT through Smad2/3 signaling pathway. *Biochem. Biophys. Res. Commun.* **528**, 545–553 (2020).
33. Wang, S., Zhao, X., Yang, S., Chen, B. & Shi, J. Knockdown of NLRC5 inhibits renal fibroblast activation via modulating TGF-β1/Smad signaling pathway. *Eur. J. Pharmacol.* **829**, 38–43 (2018).
34. Xu, T. et al. NLRC5 regulates TGF-β1-induced proliferation and activation of hepatic stellate cells during hepatic fibrosis. *Int. J. Biochem. Cell Biol.* **70**, 92–104 (2016).
35. Ma, S.-R. & Xie, X.-W. NLRC5 deficiency promotes myocardial damage induced by high fat diet in mice through activating TLR4/NF-κB. Biomedicine &amp. *Pharmacotherapy* **91**, 755–766 (2017).
36. Kuenzel, S. et al. The Nucleotide-Binding Oligomerization Domain-Like Receptor NLRC5 Is Involved in IFN-Dependent Antiviral Immune Responses. *J. Immunol.* **184**, 1990–2000 (2010).
37. Kuma, A. et al. The role of autophagy during the early neonatal starvation period. *Nature* **432**, 1032–1036 (2004).
38. Nakai, A. et al. The role of autophagy in cardiomyocytes in the basal state and in response to hemodynamic stress. *Nat. Med.* **13**, 619–624 (2007).
39. Eisenberg, T. et al. Cardioprotection and lifespan extension by the natural polyamine spermidine. *Nat. Med.* **22**, 1428–1438 (2016).
40. Hill, M. M. et al. PTRF-Cavin, a conserved cytoplasmic protein required for caveola formation and function. *Cell* **132**, 113–124 (2008).
41. Wu, Y. et al. Caveolae sense oxidative stress through membrane lipid peroxidation and cytosolic release of CAVIN1 to regulate NRF2. *Dev. Cell* **58**, 376–397.e4 (2023).
42. Kovtun, O. et al. Structural Insights into the Organization of the Cavin Membrane Coat Complex. *Dev. Cell* **31**, 405–419 (2014).
43. McMahon, K.-A. et al. Identification of intracellular cavin target proteins reveals cavin-PP1alpha interactions regulate apoptosis. *Nat. Commun.* **10**, 3279 (2019).
44. Tillu, V. A., Kovtun, O., McMahon, K.-A., Collins, B. M. & Parton, R. G. A phosphoinositide-binding cluster in cavin1 acts as a molecular sensor for cavin1 degradation. *Mol. Biol. Cell.* **26**, 3561–3569 (2015).
45. Le Lay, S. et al. The lipoatrophic caveolin-1 deficient mouse model reveals autophagy in mature adipocytes. *Autophagy* **6**, 754–763 (2010).
46. Wu, D. et al. Caveolin-1-Autophagy Pathway Mediated Cardiomyocyte Hypertrophy Induced by Apelin-13. *DNA Cell. Biol.* **36**, 611–618 (2017).
47. Shi, Y. et al. Critical role of CAV1/caveolin-1 in cell stress responses in human breast cancer cells via modulation of lysosomal function and autophagy. *Autophagy* **11**, 769–784 (2015).
48. Zhang, X. et al. Cav-1 (Caveolin-1) Deficiency Increases Autophagy in the Endothelium and Attenuates Vascular Inflammation and Atherosclerosis. *ATVB* **40**, 1510–1522 (2020).
49. Fan, Y. et al. Phosphoproteomic Analysis of Neonatal Regenerative Myocardium Revealed Important Roles of Checkpoint Kinase 1 via Activating Mammalian Target of Rapamycin C1/Ribosomal Protein S6 Kinase b-1 Pathway. *Circulation* **141**, 1554–1569 (2020).
50. Zhang, H. et al. Necroptosis mediated by impaired autophagy flux contributes to adverse ventricular remodeling after myocardial infarction. *Biochem. Pharmacol.* **175**, 113915 (2020).
51. Klionsky, D. J. et al. Guidelines for the use and interpretation of assays for monitoring autophagy (4th edition)1. *Autophagy* **17**, 1–382 (2021).
52. Smith, P. J. et al. Effects of estrogen replacement on infarct size, cardiac remodeling, and the endothelin system after myocardial infarction in ovariectomized rats. *Circulation* **102**, 2983–2989 (2000).
53. van Eickels, M. et al. 17-beta-estradiol increases cardiac remodeling and mortality in mice with myocardial infarction. *J. Am. Coll. Cardiol.* **41**, 2084–2092 (2003).
54. Li, Y. et al. Serine/Threonine-Protein Kinase 3 Facilitates Myocardial Repair After Cardiac Injury Possibly Through the Glycogen Synthase Kinase-3β/β-Catenin Pathway. *JAHA* **10**, e022802 (2021).
55. Desta, I. T., Porter, K. A., Xia, B., Kozakov, D. & Vajda, S. Performance and Its Limits in Rigid Body Protein-Protein Docking. *Structure* **28**, 1071–1081.e3 (2020).
56. Kozakov, D. et al. The ClusPro web server for protein–protein docking. *Nat. Protoc.* **12**, 255–278 (2017).
57. Ben-Kiki, O., Bercovich, A., Lifshitz, A. & Tanay, A. Metacell-2: a divide-and-conquer metacell algorithm for scalable scRNA-seq analysis. *Genome Biol.* **23**, 100 (2022).

Acknowledgements

This work was supported by grants from the Key Clinical Frontier Technology Project of Department of Science and Technology of Jiangsu Provincial (NO. BE2022806), the National Natural Science Foundation of China Innovative Research Group Project (NO. 82121001), and the Jiangsu Province Hospital (the First Affiliated Hospital of Nanjing Medical University) Clinical Capacity Enhancement Project (JSPH-MA-2021-2).

Author contributions

L.F.G. conducted the in vitro and in vivo experiments, analyzed data and wrote the manuscript. S.B.W. and L.H.Z. conducted the in vivo experiments and editing the manuscript. W.J.W and Y.L.B performed some of the in vitro experiments and editing the manuscript. Y.H., T.T.Y., J.T.S., and Q.Q.J. participated in some in vivo experiments. T.K.S. and C.D. participated in the statistical analysis and analyzed data. Z.M.W. and H.W. helped with experimental design and study guidance. L.P.X., A.H.G., Y.Z., and Y.J. participated in the editing of the manuscript and study guidance. Q.M.W. and L.S.W. supervised and managed the whole study. All authors have read and approved the final submitted manuscript.

Competing interests

The authors declare no competing interests.

Ethics approval

The manuscript does not contain clinical studies or patient data. All animal experiments in this study were performed in conformity with the Guide for the Care and Use of Laboratory Animals published by the National Institutes of Health (NIH, 2011), and were approved by the Animal Management and Use Committee and authorized by the Animal Ethics Committee of Nanjing Medical University (NO. 2403035). We have complied with all relevant ethical regulations for animal use.

Additional information

Supplementary information The online version contains supplementary material available at https://doi.org/10.1038/s42003-025-07755-z.

Correspondence and requests for materials should be addressed to Qiming Wang or Liansheng Wang.

Peer review information *Communications Biology* thanks Jianhui Zhuang and the other, anonymous, reviewer(s) for their contribution to the peer review of this work. Primary Handling Editor: Christina Karlsson Rosenthal. A peer review file is available.